

Non-global Structure of the $\mathcal{O}(\alpha_s^2)$ Dijet Soft Function

Andrew Hornig

University of Washington, Seattle, WA 98195-1560, USA

E-mail: ahornig@uw.edu

Christopher Lee¹ and Iain W. Stewart^{1,2}

¹Center for Theoretical Physics, Massachusetts Institute of Technology, Cambridge, MA 02139, USA

²Center for the Fundamental Laws of Nature, Harvard University, Cambridge, MA 02138, USA

E-mail: cleel37@mit.edu, iains@mit.edu

Jonathan R. Walsh and Saba Zuberi

Theoretical Physics Group, Ernest Orlando Lawrence Berkeley National Laboratory, and Center for Theoretical Physics, University of California, Berkeley, CA 94720, USA

E-mail: jwalsh@lbl.gov, szuberi@lbl.gov

ABSTRACT:

High energy scattering processes involving jets generically involve matrix elements of light-like Wilson lines, known as soft functions. These describe the structure of soft contributions to observables and encode color and kinematic correlations between jets. We compute the dijet soft function to $\mathcal{O}(\alpha_s^2)$ as a function of the two jet invariant masses, focusing on terms not determined by its renormalization group evolution that have a non-separable dependence on these masses. Our results include non-global single and double logarithms, and analytic results for the full set of non-logarithmic contributions as well. Using a recent result for the thrust constant, we present the complete $\mathcal{O}(\alpha_s^2)$ soft function for dijet production in both position and momentum space. We also show numerically that in certain kinematic situations hard radiation provides an additional source of non-global double and single logarithms.

KEYWORDS: Jets, Wilson Lines, Eikonal Cross Sections, Perturbative QCD.

Contents

| | |
|--|-----------|
| 1. Introduction | 2 |
| 2. The Dijet Hemisphere Soft Function | 7 |
| 2.1 Definitions | 7 |
| 2.2 Renormalization Group and Exponentiation Constraints | 8 |
| 2.3 Numerical Results for Thrust and Heavy Jet Mass Projections | 9 |
| 2.4 Non-Global Logs from $S(x_1, x_2, \mu)$ | 10 |
| 2.5 Hoang-Kluth Ansatz | 11 |
| 3. Calculation of the Dijet Hemisphere Soft Function | 11 |
| 3.1 $\mathcal{O}(\alpha_s)$ Results | 14 |
| 3.2 Structure of the $\mathcal{O}(\alpha_s^2)$ Real and Virtual Terms | 15 |
| 3.3 Final Dijet Hemisphere Soft Functions | 17 |
| 3.3.1 Result in Position Space | 18 |
| 3.3.2 Result in Momentum Space | 20 |
| 4. Projection onto Other Observables | 23 |
| 4.1 The Double Cumulant of the Non Global Terms | 23 |
| 4.2 Asymmetric Heavy Jet Mass and Asymmetric Thrust | 25 |
| 4.2.1 Projection for the Non-Global Terms from Position Space | 25 |
| 4.2.2 Projection from Momentum Space | 26 |
| 4.3 Heavy Jet Mass and Thrust | 27 |
| 4.3.1 Projection From Position Space | 27 |
| 4.3.2 Projection from Momentum Space | 28 |
| 5. Two Dimensional Comparison with EVENT2 | 29 |
| 5.1 Soft Non-Global Logarithms | 29 |
| 5.2 Hard Non-Global Logarithms | 32 |
| 6. Conclusions, Simple Generalizations, and Outlook | 34 |
| A. Anomalous Dimensions | 36 |
| B. $\mathcal{O}(\alpha_s^2)$ Diagram Results for the Opposite Hemisphere Soft Function | 37 |
| B.1 Form of the Matrix Elements in Momentum and Position Space | 40 |
| B.2 \mathcal{I} and \mathcal{T} diagrams | 42 |
| B.3 \mathcal{G} and \mathcal{H} diagrams | 43 |
| B.4 \mathcal{Q} diagrams | 45 |
| B.5 Total Opposite Hemisphere Soft Functions | 46 |

1. Introduction

Jets play a ubiquitous role at all high-energy colliders, both as signals for new particles which interact strongly, and as backgrounds for such signals through Standard Model processes involving the strong interactions. Thus it is crucial to achieve reliable and precise theoretical predictions for many types of jet cross sections.

Two obstacles to achieving precision predictions for jet observables are poor behavior of perturbative expansions and uncontrolled nonperturbative corrections. Two key tools for overcoming these challenges are factorization and resummation of large logarithms [1]. For a jet cross section which factorizes, the separation of perturbative and nonperturbative corrections increases the predictive power thanks to universality of the nonperturbative contributions, and the perturbative contributions can be organized according to the different dynamical scales (e.g. hard, jet, soft) contributing to the cross section. The presence of these disparate scales allows factorization but is also the culprit in producing large logarithms in perturbative results for jet cross sections. Techniques to resum these logarithms to all orders in perturbation theory are often critical to obtaining well-behaved predictions.

The most powerful methods to resum such logarithms rely on the renormalization group evolution of the different factors that appear in a factorized jet cross section, which are separated at an arbitrary scale μ . Such methods have been developed directly within the language of perturbative QCD itself [2, 3, 4]. An alternative approach has been formulated in the powerful language of the soft-collinear effective field theory (SCET) [5, 6, 7, 8, 9]. For e^+e^- annihilation cross sections in which the jet-like structure of an entire event is probed with a single (“global”) variable, such as thrust [10], heavy jet mass [11], angularities [12], etc., these methods succeed in resumming all logarithms of the “event shape” that become large in the two-jet limit to a well defined order in resummed perturbation theory [2, 3, 12, 13, 14, 15, 16, 17, 18]. For such a global two-jet event shape, e , the cross section takes the form $d\sigma/de = d\sigma/de|_{\text{dijet}}[1 + O(e)]$, where the leading order piece factorizes schematically as [12, 19],

$$\left. \frac{d\sigma}{de} \right|_{\text{dijet}} = \sigma_0 H(Q; \mu) [J_n(Qe^{1/j}; \mu) \otimes J_{\bar{n}}(Qe^{1/j}; \mu) \otimes S(Qe; \mu)], \quad (1.1)$$

in terms of a hard function H , jet functions $J_{n,\bar{n}}$, and soft function S . The \otimes denotes convolutions in the e -dependent arguments of $J_{n,\bar{n}}$ and S . For event shapes like thrust and jet mass, the exponent $j = 2$, but for angularities, j takes a range of values greater than 1. σ_0 is the total Born cross-section. Each function depends on logs only of a single ratio of scales, μ/Q for H , $\mu/(Qe^{1/j})$ for J , and $\mu/(Qe)$ for S . Solving the renormalization group evolution equations in μ for each of these functions produces a form for $d\sigma/de$ in which all large logarithms of e are resummed to a given order in resummed perturbation theory. The same technology can also be used to factorize and resum cumulative distributions or “cumulant” observables,

$$\Sigma(e_c) = \int_0^{e_c} de \frac{d\sigma}{de}. \quad (1.2)$$

As a step towards more exclusive probes of jets than Eq. (1.1), we can consider cross sections differential in more than one measure of the “jettiness” of a final state. We

will focus here on the particular example of dijet cross sections in the context of e^+e^- annihilation at center-of-mass energy Q , in particular, the dijet invariant mass distribution to hadronic final states X defined by

$$\begin{aligned} \frac{d\sigma}{dm_1^2 dm_2^2} &= \frac{1}{2Q^2} \sum_X |\langle X | j^\mu L_\mu | 0 \rangle|^2 (2\pi)^4 \delta^4(Q - p_X) \\ &\times \delta\left(m_1^2 - \left(\sum_{i \in L} p_i\right)^2\right) \delta\left(m_2^2 - \left(\sum_{i \in R} p_i\right)^2\right), \end{aligned} \quad (1.3)$$

where j^μ and L_μ are sums of the vector and axial currents in QCD and QED, respectively. L, R are the two hemispheres defined with respect to the thrust axis of the final state X , and p_i is the four-momentum of the i th particle in L, R . Using the formalism of SCET [5, 6, 7, 8], it has been shown that this cross section factorizes into the form [15, 13],

$$\frac{d\sigma}{dm_1^2 dm_2^2} = \sigma_0 H(Q, \mu) \int d\ell_1 d\ell_2 J_n(m_1^2 - Q\ell_1, \mu) J_{\bar{n}}(m_2^2 - Q\ell_2, \mu) S(\ell_1, \ell_2, \mu) + \dots, \quad (1.4)$$

to all orders in α_s . The ellipses denote that the result is at leading order in the power expansion in $m_{1,2}^2/Q^2 \ll 1$. The corresponding factorization theorem for the double cumulant $\Sigma(m_1^{c2}, m_2^{c2}) = \int dm_1^2 dm_2^2 \theta(m_1^{c2} - m_1^2) \theta(m_2^{c2} - m_2^2) d^2\sigma/(dm_1^2 dm_2^2)$ is

$$\Sigma(m_1^{c2}, m_2^{c2}) = \sigma_0 H(Q, \mu) Q^2 \int d\ell_1^c d\ell_2^c J_n(m_1^{c2} - Q\ell_1^c, \mu) J_{\bar{n}}(m_2^{c2} - Q\ell_2^c, \mu) \mathcal{S}_c(\ell_1^c, \ell_2^c, \mu) + \dots, \quad (1.5)$$

where \mathcal{S}_c is the double cumulant soft function

$$\mathcal{S}_c(\ell_1^c, \ell_2^c, \mu) = \int^{\ell_1^c} d\ell_1 \int^{\ell_2^c} d\ell_2 S(\ell_1, \ell_2, \mu). \quad (1.6)$$

Eqs. (1.4) and (1.5) exhibit a richer structure than Eq. (1.1), containing more information about the two-jet-like final state, and presenting additional challenges to resumming all potentially large logarithms. Each of the hard and jet functions depend only on ratios of μ to a single scale, Q or m_i , but in contrast to Eq. (1.1) the soft function now depends on the ratios μ/ℓ_1 , μ/ℓ_2 , and ℓ_1/ℓ_2 . When $m_1 \sim m_2$ the factorization theorem Eqs. (1.4) and (1.5) allow resummation of logs of m_1/Q and m_2/Q to arbitrarily high accuracy. Since it leaves logs of m_1/m_2 in fixed order perturbation theory without resummation, it does not handle log resummation for $m_1 \gg m_2$. In the latter situation hierarchies appear in the ratios appearing in the hemisphere soft function. These latter logs are examples of what have been dubbed “non-global logarithms” (NGLs) [20].

At present, all of the ingredients in Eq. (1.4) are known analytically at $\mathcal{O}(\alpha_s^2)$ except for the soft function $S(\ell_1, \ell_2, \mu)$. What is known so far about S at this order are all the logs of μ/ℓ_1 and μ/ℓ_2 thanks to knowledge of the anomalous dimensions to two-loop order (the cusp anomalous dimension is known to three-loop order). These terms are constrained by renormalization group invariance of the physical cross section Eq. (1.4), requiring the sum of the anomalous dimensions of $H, J_n, J_{\bar{n}}$, and S to add to zero. What is not known are the functions of ℓ_1/ℓ_2 that can arise in S at $\mathcal{O}(\alpha_s^2)$. Conjectures have been made about what

types of functions can arise [21], but these have never been validated nor their coefficients calculated analytically.

Knowledge of the soft function $S(l_1, l_2, \mu)$ is applicable not only in the dijet invariant mass distribution Eq. (1.4) itself, but also to a wide class of event shapes in e^+e^- annihilation, including thrust, heavy jet mass, and the “asymmetric” thrust and jet mass variables [21]. Knowledge of S to $\mathcal{O}(\alpha_s^2)$ is required to achieve NNLL (and higher) accuracy in resummed predictions for distributions in these observables, and is important input for recent extractions of the strong coupling α_s at N³LL from thrust [16, 18] and the heavy jet mass [22]. These analyses currently depend on numerical extraction of $\mathcal{O}(\alpha_s^2)$ constants from the Monte Carlo generator EVENT2 [23, 24]. The same S also enters event shape distributions for massive jets [13, 15], applicable for example for extracting the top quark mass from jet mass distributions. Although Eq. (1.4) is formulated for e^+e^- collisions, the hemisphere dijet soft function is actually closely related to an incoming dijet soft function that appears in event shapes for hadron-hadron collisions, such as the “beam thrust” or “0-jettiness” cross sections introduced in [25, 26]. In that case, the two masses are those of the measured radiation in hemispheres determined by the beam directions.

Observables like the dijet invariant mass distribution can probe the jet-like structure of an event in a “non-global” way, meaning that they are sensitive to soft radiation at different scales in sharply divided regions of phase space. The remaining sensitivity to these scales in the soft functions produces NGLs. Other examples of such non-global observables are exclusive jet cross sections [27] and jet shape distributions [28, 29] using particular jet algorithms, as well as distributions from jet substructure algorithms [30]. Accounting for and resumming these logarithms will be important for achieving precision jet phenomenology in this era where we probe jets with ever more exclusive measures.

NGLs thus far have not been resummed using the renormalization group-based techniques mentioned above. Their presence was first pointed out by Dasgupta and Salam in [20]. In that paper, they actually considered the cumulative *single*-hemisphere invariant mass distribution $\Sigma(\rho_R)$, related to our dijet invariant mass distribution Eq. (1.4) by

$$\Sigma(\rho_R) = \int_0^\infty dm_1^2 \int_0^{Q^2 \rho_R} dm_2^2 \frac{d\sigma}{dm_1^2 dm_2^2}. \quad (1.7)$$

Dasgupta and Salam noted (in our language¹) that a prediction for $\Sigma(\rho_R)$ based on inserting the dijet factorization theorem Eq. (1.4) in the relation Eq. (1.7) would not resum all logs of ρ_R from renormalization group evolution. Resummed results therefore need to be supplemented by a factor containing the NGLs,

$$\Sigma(\rho_R) = \Sigma_{\text{resum}}^{\text{dijet}}(\rho_R) \left[1 - \frac{\alpha_s^2 C_F C_A \pi^2}{(2\pi)^2} \frac{1}{3} \ln^2 \left(\frac{1}{\rho_R} \right) + \dots \right]. \quad (1.8)$$

They identified the physical source of these additional logarithms as soft gluons. Now, it is not immediately obvious that it is sufficient to consider only soft gluons when calculating

¹In the original language of [20], the resummed prediction was based on the Catani-Trentadue quark “jet” functions Σ_q defined by [31, 32] for use in resumming logs in global two-jet event shape distributions.

$\Sigma(\rho_R)$, since the radiation in the left hemisphere is allowed to become hard. The good agreement in [20] between the coefficient of the NGL in Eq. (1.8) and their numerical results from EVENT2 would suggest that this NGL does arise from two purely soft gluons going into opposite hemispheres. To be precise, we will distinguish between “hard NGLs” involving hard radiation and “soft NGLs” for which the eikonal approximation suffices. Our main focus in this paper is on obtaining analytical results for the latter. However, we find evidence numerically for such additional hard NGLs. For soft NGLs, the relation Eq. (1.7) suggests that the NGL in Eq. (1.8) found by [20] in the soft approximation can be interpreted as arising from a double log of l_1/l_2 in the fixed order $\mathcal{O}(\alpha_s^2)$ part of the soft function $S(l_1, l_2, \mu)$ in Eq. (1.4). We will use our results to verify this statement.

In this paper, we calculate the full structure of the dijet soft function $S(l_1, l_2, \mu)$ at $\mathcal{O}(\alpha_s^2)$ analytically, and also explore the relation to NGLs, which first arise at this order. We will learn that NGLs of a given observable can be understood as logs of ratios of multiple soft scales that are left over in the perturbative expansion of the relevant soft function even after a factorization theorem for the observable has been established. This perspective allows one to calculate systematically not only the leading non-global logarithms that have been identified in [20], but also to calculate straightforwardly the full set of other non-global structures that actually arise.

We will find it simpler for many purposes to work with the Fourier transform of $S(l_1, l_2, \mu)$ to position space. The cross section transforms as

$$\tilde{\sigma}(y_1, y_2) = \int_{-\infty}^{\infty} dm_1^2 dm_2^2 e^{-im_1^2 y_1} e^{-im_2^2 y_2} \sigma(m_1^2, m_2^2, \mu). \quad (1.9)$$

In position space, the convolution in Eq. (1.4) becomes a product,

$$\tilde{\sigma}(y_1, y_2) = \sigma_0 H_2(Q; \mu) \tilde{J}_n(y_1, \mu) \tilde{J}_{\bar{n}}(y_2, \mu) \tilde{S}(Qy_1, Qy_2, \mu). \quad (1.10)$$

In position space, the renormalization group evolution of each factor becomes particularly simple as they each renormalize multiplicatively, as opposed to convolutions in momentum space. In fact, RGEs in momentum space are most easily solved by first going through position space [33, 34], and there are several formalisms on the market to do this to arbitrary high orders as long as the anomalous dimensions are known (using derivatives on the evolution kernels [35], converting analytically back to momentum space [36], or even transforming numerically). For example, the derivative formalism of [35] for summing logarithms in momentum space relies on the form of the position (or Laplace)-space soft function (the “associated jet/soft functions” in [35]). Thus the position space soft function $\tilde{S}(x_1, x_2, \mu)$ is a crucial ingredient in resummation of logs in practically all dijet observables.

We will present results for the dijet soft function to $\mathcal{O}(\alpha_s^2)$ both in position space, $\tilde{S}(x_1, x_2, \mu)$, and for the double cumulant in momentum space, $\mathcal{S}_c(\ell_1^c, \ell_2^c, \mu)$. We determine analytically for the first time the full set of functions of x_1/x_2 or ℓ_1^c/ℓ_2^c that appear in \tilde{S} and \mathcal{S}_c at this order.²

From our results, we learn:

²There is a constant term in $\tilde{S}(x_1, x_2, \mu)$, or coefficient of $\delta(l_1)\delta(l_2)$ in $S(l_1, l_2, \mu)$, that we do not calculate, but which can be deduced from the recent result for the thrust soft function by [37].

- There is a non-global double logarithm with $C_F C_A$ color structure in $\mathcal{S}_c(\ell_1^c, \ell_2^c, \mu)$ and $S(x_1, x_2, \mu)$, which corresponds exactly to the non-global log first identified by Dasgupta and Salam in [20] from the single hemisphere mass distribution.
- There is a single non-global logarithm in $\mathcal{S}_c(\ell_1^c, \ell_2^c, \mu)$ and $\tilde{S}(x_1, x_2, \mu)$ that appears when the ratio ℓ_1^c/ℓ_2^c or ℓ_2^c/ℓ_1^c becomes large, or when x_1/x_2 or x_2/x_1 becomes large. Both the color structures $C_F C_A$ and $C_F T_{Rn_f}$ have this single log.
- In addition, other non-logarithmic non-global structures arise in \mathcal{S}_c and \tilde{S} at $\mathcal{O}(\alpha_s^2)$. These structures and the single log were not accounted for in previous conjectures about their form [21].
- When $m_2^2 \ll m_1^2 \sim Q^2$, we demonstrate numerically in EVENT2 the existence of hard non-global logarithms in double hemisphere mass distributions that are not captured by the soft functions above or any previous results based on eikonal approximations.

These results not only complete our knowledge of the soft function at $\mathcal{O}(\alpha_s^2)$, together with known results for the hard and jet functions in Eqs. (1.4) and (1.10), they make possible resummation to N³LL accuracy in these doubly-differential cross sections when $\ell_1/\ell_2 \sim 1$ or $x_1/x_2 \sim 1$ (when these ratios are large/small the NGLs must be resummed as well). In position space the complete analytic N³LL result can immediately be obtained from our results through multiplicative RG evolution, while in momentum space convolutions between the evolution factors and fixed order functions must still be performed. This becomes a more nontrivial exercise to perform in the presence of the non-logarithmic non-global structures found here.

We arrive at the above results as follows: In Sec. 2, we review properties of the dijet soft function that are known, and a conjecture for the $\mathcal{O}(\alpha_s^2)$ parts of it that are (so far) unknown. We also explore the relation to NGLs in detail. In Sec. 3, we give our final results for the calculation of the dijet soft functions in position space, $\tilde{S}(x_1, x_2, \mu)$, and the double cumulant projection of the momentum space soft function, $\mathcal{S}_c(\ell_1^c, \ell_2^c, \mu)$, to $\mathcal{O}(\alpha_s^2)$. We organize contributions to the two-loop soft function according to whether one or both hemispheres are populated by final state particles. Thanks to renormalization group invariance and known anomalous dimensions of the two-loop soft function, we obtain all the new information we need from contributions with two particles (gluons or quark-antiquark) in the final state going into opposite hemispheres. These contributions encode all the non-global structure in the dijet soft function. In addition, we will give a remarkably simple function that approximates very closely the total non-logarithmic non-global terms in the double cumulant \mathcal{S}_c .

In Sec. 4, we discuss several projections of our soft functions $S(\ell_1, \ell_2, \mu)$ and $\tilde{S}(x_1, x_2, \mu)$, including how we obtain analytic results for the double cumulant, $\mathcal{S}_c(\ell_1^c, \ell_2^c)$, and the asymmetric thrust and heavy jet-mass event shapes of Ref. [21]. The latter include the standard thrust and heavy jet-mass projections as special cases, and we compare our analytic results to EVENT2, providing a strong consistency check. In Sec. 5 we carry out another consistency check by comparing the dijet factorization theorem with $\mathcal{S}_c(m_1^c, m_2^c)$, expanded to

$\mathcal{O}(\alpha_s^2)$, to the two-dimensional double cumulant distribution from EVENT2. We demonstrate that when our results are included in the factorization theorem in Eq. (1.4) at $\mathcal{O}(\alpha_s^2)$ that the remaining terms are truly power suppressed. In Section 6, we conclude.

In Appendix A, we record the known anomalous dimensions of the dijet soft function to two-loop order, which we need to assemble our result for the full soft function. In Appendix B, we provide details of the calculation of the various parts of the soft function given in Sec. 3, organized by color factors and Feynman diagram topologies. We give results in both momentum and position space and provide details of the translation between the two.

2. The Dijet Hemisphere Soft Function

2.1 Definitions

The dijet hemisphere soft function is defined as

$$S(\ell_1, \ell_2) = \frac{1}{N_c} \sum_{X_S} \left| \langle X_S | T[Y_n^\dagger Y_{\bar{n}}] | 0 \rangle \right|^2 \delta\left(\ell_1 - \sum_{i \in L} \bar{n} \cdot k_i\right) \delta\left(\ell_2 - \sum_{i \in R} n \cdot k_i\right), \quad (2.1)$$

where T denotes time ordering, $n^\mu = (1, 0, 0, 1)$ and $\bar{n}^\mu = (1, 0, 0, -1)$ are light-cone vectors along the $\pm z$ directions, and L, R specify the $\pm \hat{z}$ hemispheres which we refer to as left and right hemispheres. The Wilson lines $Y_{n, \bar{n}}$ are exponentials of soft gluons,

$$Y_n^\dagger = P \exp \left[ig \int_0^\infty ds n \cdot A_s(ns) \right], \quad Y_{\bar{n}} = \bar{P} \exp \left[-ig \int_0^\infty ds \bar{n} \cdot A_s(\bar{n}s) \right], \quad (2.2)$$

where P denotes path ordering for color matrices and \bar{P} denotes anti-path ordering. When deriving factorization theorems in SCET, soft Wilson lines are generated for each jet direction from rotating the collinear fields in the SCET Lagrangian to decouple soft gluon interactions with collinear quarks and gluons [8]. Equation (2.1) is referred to as a dijet soft function because Y_n^\dagger and $Y_{\bar{n}}$ Wilson lines appear from the n -jet and \bar{n} -jet, and is referred to as a hemisphere soft function because the measurement function $\mathcal{M}(\ell_1, \ell_2)$ involves kinematic variables restricted to hemispheres,

$$\mathcal{M}(\ell_1, \ell_2) = \delta\left(\ell_1 - \sum_{i \in L} \bar{n} \cdot k_i\right) \delta\left(\ell_2 - \sum_{i \in R} n \cdot k_i\right). \quad (2.3)$$

A more symmetric expression for the dijet hemisphere soft function can be obtained by converting to the $\bar{\mathbf{3}}$ representation [38]. Using $T(Y_{\bar{n}})^T = \bar{Y}_{\bar{n}}^\dagger = P \exp(ig \int_0^\infty ds \bar{n} \cdot \bar{A}_s(\bar{n}s))$ and $\bar{T}(Y_n^\dagger)^T = \bar{P} \exp(-ig \int_0^\infty ds \bar{n} \cdot \bar{A}_s(\bar{n}s))$, where $\bar{A}_\mu = \bar{T}^A A_\mu^A = -(T^A)^T A_\mu^A$, gives

$$S(\ell_1, \ell_2) = \frac{1}{N_c} \left\langle 0 \left| \text{tr} \bar{Y}_{\bar{n}}^T Y_n \mathcal{M}(\ell_1, \ell_2) Y_n^\dagger \bar{Y}_{\bar{n}}^* \right| 0 \right\rangle. \quad (2.4)$$

Due to the simple product structure of the position space factorization theorem in Eq. (1.10), it is often easier to work with the Fourier transform of $S(\ell_1, \ell_2)$,

$$\tilde{S}(x_1, x_2) = \int d\ell_1 d\ell_2 e^{-i\ell_1 x_1} e^{-i\ell_2 x_2} S(\ell_1, \ell_2). \quad (2.5)$$

The definitions in Eqs. (2.1) and (2.5) imply that the functions S and \tilde{S} are symmetric under interchange of the two hemispheres,

$$S(\ell_1, \ell_2) = S(\ell_2, \ell_1), \quad \tilde{S}(x_1, x_2) = \tilde{S}(x_2, x_1). \quad (2.6)$$

Note that the function $S(\ell_1, \ell_2)$ has naive mass dimension -2 , whereas $\tilde{S}(x_1, x_2)$ is dimensionless.

2.2 Renormalization Group and Exponentiation Constraints

Renormalization group invariance of the factorized hemisphere cross section implies a factorized structure for the soft function renormalization and its renormalization group evolution [39]. Defining counterterms Z_S in the $\overline{\text{MS}}$ scheme, the renormalized soft function which appears in the factorization theorem in Eq. (1.10) is

$$\tilde{S}(x_1, x_2, \mu) = Z_S^{-1}(x_1, \mu) Z_S^{-1}(x_2, \mu) \tilde{S}(x_1, x_2)^{\text{bare}}, \quad (2.7)$$

and its inverse Fourier transform to momentum space, $S(\ell_1, \ell_2, \mu)$, appears in the factorization theorem in Eq. (1.4). Since $\tilde{S}(x_1, x_2, \mu)$ is dimensionless it can only be a function of μx_1 , μx_2 , x_1/x_2 , and $\alpha_s(\mu)$, where the μ dependence is uniquely determined by the renormalization group. From now on we will drop the supercript “bare” for bare objects, which are always denoted without dependence on μ , and we will include μ as an argument for renormalized functions. The renormalization group equation (RGE) for \tilde{S} is

$$\begin{aligned} \mu \frac{d}{d\mu} \ln \tilde{S}(x_1, x_2, \mu) &= \gamma_S(x_1, \mu) + \gamma_S(x_2, \mu), \\ \gamma_S(x, \mu) &= -Z_S^{-1}(x, \mu) \mu \frac{d}{d\mu} Z_S(x, \mu) = -\Gamma_{\text{cusp}}[\alpha_s] \ln(i e^{\gamma_E} x \mu) + \gamma_S[\alpha_s]. \end{aligned} \quad (2.8)$$

The solution of this RGE allows \tilde{S} at μ to be expressed in terms of \tilde{S} at μ_0 ,

$$\tilde{S}(x_1, x_2, \mu) = U_S(x_1, \mu, \mu_0) U_S(x_2, \mu, \mu_0) \tilde{S}(x_1, x_2, \mu_0), \quad (2.9)$$

where

$$U_S(x, \mu, \mu_0) = e^{K(\Gamma_{\text{cusp}}, \gamma_S, \mu, \mu_0)} (i e^{\gamma_E} x \mu_0)^{\omega(\Gamma_{\text{cusp}}, \gamma_S, \mu, \mu_0)}, \quad (2.10)$$

and the functions K and ω are given in Appendix A.

Following Ref. [39] the μ dependence in Eq. (2.9) can be entirely organized into the evolution factors by writing

$$\tilde{S}(x_1, x_2, \mu) = U_S(x_1, \mu, \mu_{x_1}) U_S(x_2, \mu, \mu_{x_2}) e^{\tilde{T}(x_1, x_2)}, \quad (2.11)$$

where $\mu_{x_i} = (i e^{\gamma_E} x_i)^{-1}$ and the exponent $\tilde{T}(x_1, x_2)$ is independent of μ . In Ref. [21] Hoang and Kluth used non-Abelian exponentiation [40, 41] to show that the last factor exponentiates in this way. With μ_0 set equal to μ_{x_1} or μ_{x_2} respectively in the two evolution factors, the second factor in Eq. (2.10) dependent on ω becomes unity, and the soft function Eq. (2.11) takes the simple form

$$\tilde{S}(x_1, x_2, \mu) = e^{K_1(x_1, \mu) + K_2(x_2, \mu)} e^{\tilde{T}(x_1, x_2)}, \quad (2.12)$$

where $K_i(x_i, \mu) = K(\Gamma_{\text{cusp}}, \gamma_S, \mu, \mu_{x_i})$.

Hoang and Kluth [21] also pointed out other properties satisfied by the function $\tilde{T}(x_1, x_2)$. In particular, it is symmetric, $\tilde{T}(x_1, x_2) = \tilde{T}(x_2, x_1)$, and there are constraints on the color factors in $\tilde{T}(x_1, x_2)$ at each order in α_s . For instance, in the Abelian limit with $n_f = 0$ light quarks the function $\tilde{T}(x_1, x_2)$ is one-loop exact. At two loops the only color structures in $\tilde{T}(x_1, x_2)$ are $C_F C_A$ and $C_F T_R n_f$, where for SU(3) color the fundamental and adjoint Casimirs are $C_F = 4/3$ and $C_A = 3$, and $T_R = 1/2$. To order α_s^2 we can write

$$\tilde{T}(x_1, x_2) = \frac{\alpha_s(\mu_{x_1})}{4\pi} t_1 + \frac{\alpha_s(\mu_{x_2})}{4\pi} t_1 + 2 \frac{\alpha_s^2}{(4\pi)^2} t_2(x_1/x_2), \quad (2.13)$$

where the one-loop constant t_1 is

$$t_1 = -C_F \frac{\pi^2}{2}. \quad (2.14)$$

The dimensionless two-loop function $t_2(x_1/x_2)$ is unknown, and its computation is one of the main goals of this paper. From the symmetry $x_1 \leftrightarrow x_2$ we have $t_2(b) = t_2(1/b)$.

We will present our result for the position space soft functions by writing Eq. (2.12) as

$$\tilde{S}(x_1, x_2, \mu) = \tilde{R}(x_1, x_2, \mu) + \hat{S}(x_1, x_2), \quad (2.15)$$

where all terms containing logs of (μx_i) are grouped together into $\tilde{R}(x_1, x_2, \mu)$ and all other terms are separated into $\hat{S}(x_1, x_2)$. All quantities appearing in \tilde{R} or \hat{S} will be expanded in powers of $\alpha_s(\mu)$ [in contrast to $\alpha_s(\mu_{x_i})$ in Eq. (2.13)]. So $\tilde{R}(x_1, x_2, \mu)$ contains cross terms between the one-loop anomalous dimensions in $K_{1,2}$ and the one-loop part of $\tilde{T}(x_1, x_2)$, as well as terms generated by the running of $\alpha_s(\mu_{x_i})$ in Eq. (2.13). Similarly we will present the result for the double cumulant momentum space soft function $\mathcal{S}_c(\ell_1^c, \ell_2^c)$ defined in Eq. (1.6), by writing

$$\mathcal{S}_c(\ell_1^c, \ell_2^c, \mu) = \mathcal{R}(\ell_1^c, \ell_2^c, \mu) + \hat{\mathcal{S}}_c(\ell_1^c, \ell_2^c), \quad (2.16)$$

where $\mathcal{R}(\ell_1^c, \ell_2^c, \mu)$ contains all the logarithmic plus function distributions in μ/ℓ_1^c or μ/ℓ_2^c , and $\hat{\mathcal{S}}_c(\ell_1^c, \ell_2^c)$ everything else.³

2.3 Numerical Results for Thrust and Heavy Jet Mass Projections

Results for single differential event shape cross sections will depend on various projections of the function $t_2(b)$. In the literature results for these projections have been derived with the EVENT2 generator [23, 24]. For thrust T in $e^+e^- \rightarrow$ jets, we are only sensitive to the symmetric combination of hemisphere masses in the dijet limit, $\tau \equiv 1 - T = (m_1^2 + m_2^2)/Q^2 + \dots$, where the ellipses denote terms that are power corrections to the dijet factorization theorem. The relevant projection from $t_2(b)$ for thrust is

$$t_2(1) = C_F C_A s_2^{[C_F C_A]} + C_F T_R n_f s_2^{[n_f]}, \quad (2.17)$$

³Due to some constant μ -independent terms \mathcal{R} and $\hat{\mathcal{S}}_c$ are not separately related to the inverse Fourier transform of \tilde{R} and \hat{S} in Eq. (2.15), but can be obtained from these transforms by inspecting the results.

and these $s_2^{[a]}$'s contributes to the $\alpha_s^2 \delta(\tau)$ term in momentum space. Numerical determinations using EVENT2 in the literature include

$$\begin{aligned}
\text{Becher \& Schwartz [16]} : \quad & s_2^{[C_F C_A]} = -30.0 \pm 0.5, & s_2^{[n_f]} &= 21.5 \pm 0.5, \\
\text{Hoang \& Kluth [21]} : \quad & s_2^{[C_F C_A]} = -29.4 \pm 1.1, & s_2^{[n_f]} &= 21.9 \pm 1.5, \\
\text{Chien \& Schwartz [22]} : \quad & s_2^{[C_F C_A]} = -28.9, & s_2^{[n_f]} &= 21.7, \\
\text{AHMSS [42]} : \quad & s_2^{[C_F C_A]} = -28.33 \pm 0.11, & s_2^{[n_f]} &= 21.82_{-0.11}^{+0.02}.
\end{aligned} \tag{2.18}$$

Recently the two thrust constants have been computed directly by Luisoni and Monni, giving [37]

$$s_2^{[C_F C_A]} = -28.242 \pm 0.003, \quad s_2^{[n_f]} = 21.692 \pm 0.003. \tag{2.19}$$

For our analysis we will treat these two constants as known quantities.

Another event shape of interest is the heavy jet mass, $\rho_H \equiv \max(m_1^2, m_2^2)/Q^2$. In this case the only projection of $t_2(b)$ that appears at $\mathcal{O}(\alpha_s^2)$ is [22]

$$\int_0^\pi \frac{d\theta}{\pi} t_2(e^{i\theta}) = C_F C_A s_{2\rho}^{[C_F C_A]} + C_F T_R n_f s_{2\rho}^{[n_f]}. \tag{2.20}$$

We will provide an alternate derivation of the integral moment appearing in Eq. (2.20) in Sec. 4. Numerical EVENT2 results include

$$\begin{aligned}
\text{Chien \& Schwartz [22]} : \quad & s_{2\rho}^{[C_F C_A]} = -16.6, & s_{2\rho}^{[n_f]} &= 25.1, \\
\text{AHMSS [42]} : \quad & s_{2\rho}^{[C_F C_A]} = -16.79 \pm 0.46, & s_{2\rho}^{[n_f]} &= 25.15_{-0.05}^{+0.08}.
\end{aligned} \tag{2.21}$$

One of the benefits of our analytic results for $t_2(b)$ is that one can compute results for the constants appearing in various event shapes directly. In this vein in Sec. 4.2 we use our results to obtain analytic results for the combination

$$\int_0^\pi \frac{d\theta}{\pi} [t_2(e^{i\theta}) - t_2(1)] = (s_{2\rho}^{[C_F C_A]} - s_2^{[C_F C_A]}) + (s_{2\rho}^{[n_f]} - s_2^{[n_f]}). \tag{2.22}$$

Comparison of this combination with EVENT2 will provide a nontrivial cross-check on our calculations and we quote results here for easy reference

$$\begin{aligned}
\text{CS[22] - LM[37]} : \quad & (s_{2\rho} - s_2)^{[C_F C_A]} = 11.64, & (s_{2\rho} - s_2)^{[n_f]} &= 3.41. \\
\text{AHMSS[42] - LM[37]} : \quad & (s_{2\rho} - s_2)^{[C_F C_A]} = 11.55 \pm 0.46, & (s_{2\rho} - s_2)^{[n_f]} &= 3.46_{-0.05}^{+0.08}.
\end{aligned} \tag{2.23}$$

2.4 Non-Global Logs from $S(x_1, x_2, \mu)$

In this section we make the connection between calculations of non-global logarithms and logarithmic terms in the function $t_2(x_1/x_2)$. The possible form of $t_2(x_1/x_2)$ becomes simpler if we make a power expansion about the non-global limit, $x_1 \gg x_2$, which can at most

yield logarithmic singularities. The leading singularity is related to the non-global double logarithm of Ref. [20]. This expansion therefore yields

$$\lim_{x_1 \gg x_2} t_2(x_1, x_2) = s_2^{[2]} \ln^2\left(\frac{x_1}{x_2}\right) + s_2^{[1]} \ln\left(\frac{x_1}{x_2}\right) + s_2^{[0]} + \dots \quad (2.24)$$

where the terms in ellipses are suppressed by at least one power of x_1/x_2 . Since the limit is not symmetric in x_1 and x_2 , the odd power $\ln(x_1/x_2)$ can appear. In fact the coefficient $s_2^{[2]}$ can be extracted from the non-global double logarithm computed in Ref. [20]. To derive this relation note that the double cumulant invariant mass distribution is

$$\frac{1}{\sigma_0} \Sigma(m_1^{c2}, m_2^{c2}) = 1 + \dots + \frac{\alpha_s^2 s_2^{[2]}}{8\pi^2} \left[\ln^2 \frac{m_1^{c2}}{Q^2} - 2 \ln \frac{m_1^{c2}}{Q^2} \ln \frac{m_2^{c2}}{Q^2} + \ln^2 \frac{m_2^{c2}}{Q^2} \right] + \dots, \quad (2.25)$$

where only the term involving $s_2^{[2]}$ is shown. In the limit $Q^2 \gg m_2^{c2} \gg m_1^{c2}$ the $\ln^2(m_1^{c2}/Q^2)$ term is leading, and must correspond with the double logarithm of Ref. [20] since it was derived in precisely this limit. The Dasgupta and Salam calculation therefore gives $s_2^{[2]} = -2C_F C_A \pi^2/3$, or for the coefficients of the two possible color structures

$$s_2^{[2][C_F C_A]} = -\frac{2\pi^2}{3} = -6.580, \quad s_2^{[2][n_f]} = 0. \quad (2.26)$$

2.5 Hoang-Kluth Ansatz

Hoang and Kluth [21] argued that $t_2(x_1/x_2)$ should only contain powers of $\ln(x_1/x_2)$ based on the expectation that event shape distributions should contain only delta functions and plus distributions in the dijet limit. The log powers must then be even powers to satisfy the $x_1 \leftrightarrow x_2$ symmetry and known LL results constrain the largest power to $\ln^2(x_1/x_2)$ at $\mathcal{O}(\alpha_s^2)$. This led Ref. [21] to make the ansatz

$$t_2^{\text{ansatz}}(x_1/x_2) = s_2^{[2]} \ln^2\left(\frac{x_1}{x_2}\right) + s_2, \quad (2.27)$$

with two constants, s_2 for thrust, and $s_2^{[2]}$ for the double log coefficient. With this form the constant $s_2^{[2]}$ can be determined by knowing the $\mathcal{O}(\alpha_s^2)$ δ -function constants for thrust and the heavy jet-mass, via $s_2^{[2]} = 3(s_2 - s_{2\rho})/\pi^2$. The numerical results in Eq. (2.23) give $s_2^{[2][C_F C_A]} = -3.5 \pm 0.1$ and $s_2^{[2][n_f]} = -1.02 \pm 0.04$. These results differ from those in Eq. (2.26), so either the ansatz is incomplete or the calculation of Ref. [20] is missing a source of double logarithms. Using our full computation of $t_2(x_1/x_2)$ we will show that it is the ansatz in Eq. (2.27) that is incomplete. This implies that non-logarithmic terms contribute to the integral in Eq. (2.22). Expanding our $t_2(x_1/x_2)$ for $x_1 \gg x_2$ we exactly reproduce the result for $s_2^{[2]}$ in Eq. (2.26), and derive non-zero results for the coefficients $s_2^{[1]}$ and $s_2^{[0]}$.

3. Calculation of the Dijet Hemisphere Soft Function

In this section we calculate the dijet hemisphere soft function in both position space, $\tilde{S}(x_1, x_2, \mu)$, and momentum space, $S(\ell_1, \ell_2, \mu)$, to $\mathcal{O}(\alpha_s^2)$. To make the α_s expansion we

write

$$\begin{aligned}\tilde{S}(x_1, x_2, \mu) &= 1 + \tilde{S}_1(x_1, x_2, \mu) + \tilde{S}_2(x_1, x_2, \mu) + \mathcal{O}(\alpha_s^3), \\ S(\ell_1, \ell_2, \mu) &= \delta(\ell_1)\delta(\ell_2) + S_1(\ell_1, \ell_2, \mu) + S_2(\ell_1, \ell_2, \mu) + \mathcal{O}(\alpha_s^3),\end{aligned}\tag{3.1}$$

where \tilde{S}_i and S_i are the $\mathcal{O}(\alpha_s^i)$ terms. For nonzero ℓ_i or x_i the final results for each \tilde{S}_i and S_i are IR finite (see [43]). We regulate the UV divergences in $d = 4 - 2\epsilon$ dimensions and renormalize with $\overline{\text{MS}}$. In momentum space the renormalization occurs through a convolution, while it is a product in position space:

$$\begin{aligned}S(\ell_1, \ell_2) &= \int d\ell'_1 d\ell'_2 Z(\ell_1 - \ell'_1, \ell_2 - \ell'_2, \mu) S_{\text{ren}}^{(1)}(\ell'_1, \ell'_2, \mu), \\ S(x_1, x_2) &= Z(x_1, x_2, \mu) S(x_1, x_2, \mu).\end{aligned}\tag{3.2}$$

For the counterterms

$$Z(x_1, x_2, \mu) = Z(x_1, \mu)Z(x_2, \mu), \quad Z(\ell_1, \ell_2, \mu) = Z(\ell_1, \mu)Z(\ell_2, \mu),\tag{3.3}$$

we have similar α_s expansion formulae,

$$\begin{aligned}Z(x, \mu) &= 1 + Z_1(x, \mu) + Z_2(x, \mu) + \mathcal{O}(\alpha_s^3), \\ Z(\ell, \mu) &= \delta(\ell) + Z_1(\ell, \mu) + Z_2(\ell, \mu) + \mathcal{O}(\alpha_s^3).\end{aligned}\tag{3.4}$$

The calculations can be organized by the number of cut propagators,

$$\mathcal{C}(k) = 2\pi \delta(k^2) \theta(k^0).\tag{3.5}$$

At $\mathcal{O}(\alpha_s)$ we have zero or one $\mathcal{C}(k)$ for the virtual and real emission graphs respectively. The $\mathcal{O}(\alpha_s)$ matrix elements are straightforward to calculate and we give the results in Sec. 3.1. At $\mathcal{O}(\alpha_s^2)$ we have 0, 1, or 2 factors of \mathcal{C} . The general structure of the calculation is explored in Sec. 3.2, where we show that it suffices to compute the double cut graphs since the remaining terms are determined entirely by the renormalization group and the constant s_2 . Final results for $S(\ell_1, \ell_2, \mu)$ and $S(x_1, x_2, \mu)$ at $\mathcal{O}(\alpha_s^2)$ are given in Sec. 3.3, while the details of the calculation are described extensively in Appendix B.

For easy reference we also record here the form of the hemisphere measurement functions in momentum and position space, $\mathcal{M}_{\{k\}}^{[j]}(\ell_1, \ell_2)$ and $\mathcal{M}_{\{k\}}^{[j]}(x_1, x_2)$ for $j = 0, 1, 2$ final state particles with momenta k_i . It is the measurement functions that introduce the ℓ_1, ℓ_2 or $x_{1,2}$ dependence into the soft function. With no final state particle we have a tree level or purely virtual contribution and Eq. (2.3) gives

$$\mathcal{M}^{[0]}(\ell_1, \ell_2) = \delta(\ell_1)\delta(\ell_2), \quad \mathcal{M}^{[0]}(x_1, x_2) = 1.\tag{3.6}$$

For one final state particle of momentum k we have in momentum space

$$\begin{aligned}\mathcal{M}_k^{[1]}(\ell_1, \ell_2) &= \delta(\ell_1 - k^-)\delta(\ell_2)\theta(k^+ - k^-) + \delta(\ell_2 - k^+)\delta(\ell_1)\theta(k^- - k^+) \\ &= \mathcal{M}_k^{[L]}(\ell_1)\delta(\ell_2) + \delta(\ell_1)\mathcal{M}_k^{[R]}(\ell_2),\end{aligned}\tag{3.7}$$

and in position space

$$\begin{aligned}\mathcal{M}_k^{[1]}(x_1, x_2) &= e^{-ix_1 k^-} \theta(k^+ - k^-) + e^{-ix_2 k^+} \theta(k^- - k^+) \\ &= \mathcal{M}_k^{[L]}(x_1) + \mathcal{M}_k^{[R]}(x_2).\end{aligned}\tag{3.8}$$

Eqs. (3.7) and (3.8) show that the measurement divides into two terms, the contribution when the parton is in the left hemisphere plus the contribution when the parton is in the right hemisphere.

For two final state particles of momentum k_1 and k_2 we have contributions from both particles in the left hemisphere, both in the right hemisphere, or one in each hemisphere

$$\begin{aligned}\mathcal{M}_{k_1, k_2}^{[2]}(\ell_1, \ell_2) &= \mathcal{M}_{k_1, k_2}^{[LL]}(\ell_1) \delta(\ell_2) + \delta(\ell_1) \mathcal{M}_{k_1, k_2}^{[RR]}(\ell_2) + \mathcal{M}_{k_1, k_2}^{[LR]}(\ell_1, \ell_2), \\ \mathcal{M}_{k_1, k_2}^{[2]}(x_1, x_2) &= \mathcal{M}_{k_1, k_2}^{[LL]}(x_1) + \mathcal{M}_{k_1, k_2}^{[RR]}(x_2) + \mathcal{M}_{k_1, k_2}^{[LR]}(x_1, x_2).\end{aligned}\tag{3.9}$$

For two particles in the left hemisphere the functions are

$$\begin{aligned}\mathcal{M}_{k_1, k_2}^{[LL]}(\ell_1) &= \delta(\ell_1 - k_1^- - k_2^-) \theta(k_1^+ - k_1^-) \theta(k_2^+ - k_2^-), \\ \mathcal{M}_{k_1, k_2}^{[LL]}(x_1) &= e^{-ix_1(k_1^- + k_2^-)} \theta(k_1^+ - k_1^-) \theta(k_2^+ - k_2^-),\end{aligned}\tag{3.10}$$

and there is a trivial dependence on ℓ_2 or x_2 . Similarly for two particles in the right hemisphere we have

$$\begin{aligned}\mathcal{M}_{k_1, k_2}^{[RR]}(\ell_2) &= \delta(\ell_2 - k_1^+ - k_2^+) \theta(k_1^- - k_1^+) \theta(k_2^- - k_2^+), \\ \mathcal{M}_{k_1, k_2}^{[RR]}(x_2) &= e^{-ix_2(k_1^+ + k_2^+)} \theta(k_1^- - k_1^+) \theta(k_2^- - k_2^+),\end{aligned}\tag{3.11}$$

with a trivial dependence on ℓ_1 or x_1 . For one particle in each hemisphere we have

$$\begin{aligned}\mathcal{M}_{k_1, k_2}^{[LR]}(\ell_1, \ell_2) &= \delta(\ell_1 - k_1^-) \delta(\ell_2 - k_2^+) \theta(k_1^+ - k_1^-) \theta(k_2^- - k_2^+) \\ &\quad + \delta(\ell_1 - k_2^-) \delta(\ell_2 - k_1^+) \theta(k_1^- - k_1^+) \theta(k_2^+ - k_2^-), \\ \mathcal{M}_{k_1, k_2}^{[LR]}(x_1, x_2) &= e^{-ix_1 k_1^- - ix_2 k_2^+} \theta(k_1^+ - k_1^-) \theta(k_2^- - k_2^+) \\ &\quad + e^{-ix_1 k_2^- - ix_2 k_1^+} \theta(k_1^- - k_1^+) \theta(k_2^+ - k_2^-).\end{aligned}\tag{3.12}$$

Diagrams involving $\mathcal{M}^{[LR]}$ are the only ones that can simultaneously depend on ℓ_1 and ℓ_2 and hence on ℓ_1/ℓ_2 . We will exploit this further in Sec. 3.2. We will label the different graphs by the locations of the cut partons. We call the diagrams where the final state partons are all in the left hemisphere or all in the right hemisphere the *same hemisphere* terms, and we call diagrams with one parton in the left hemisphere and one parton in the right hemisphere the *opposite hemisphere* terms.

Finally we summarize some notation that will be used extensively below. In momentum space the logarithms are distributions

$$\mathcal{L}_k(t) = \left[\frac{\ln^k t}{t} \right]_+, \tag{3.13}$$

while for cumulant momentum space the logarithms are

$$L_1 \equiv \ln(\ell_1^c/\mu), \quad L_2 \equiv \ln(\ell_2^c/\mu). \quad (3.14)$$

In position space we denote the μ dependent logarithms as

$$\tilde{L}_1 \equiv \ln(ie^{\gamma_E} x_1 \mu), \quad \tilde{L}_2 \equiv \ln(ie^{\gamma_E} x_2 \mu). \quad (3.15)$$

The non-global structure of the soft function will appear through the variables.

$$r = \frac{\ell_1}{\ell_2}, \quad \text{or} \quad b = \frac{x_1}{x_2}, \quad \text{or} \quad a = \frac{\ell_1^c}{\ell_2^c}. \quad (3.16)$$

3.1 $\mathcal{O}(\alpha_s)$ Results

The $\mathcal{O}(\alpha_s)$ diagrams contribute to the $\mathcal{O}(\alpha_s^2)$ terms, so we give them explicitly. Here the soft gluon can either be real or virtual. Purely virtual diagrams (no partons cut) in the soft function are scaleless in pure dimensional regularization, so we do not need to compute them. These graphs convert all $1/\epsilon_{\text{IR}}$'s in the real emission result into $1/\epsilon_{\text{UV}}$'s. A demonstration of this which applies to our calculation here was given in Refs. [17, 44]. The measurement function $\mathcal{M}_k^{(1)}(\ell_1, \ell_2)$ in Eq. (3.7) divides the calculation into two terms, one coming from the gluon in the left hemisphere and one coming from the gluon in the right hemisphere.

The bare one loop soft function in momentum space and position space in dimensional regularization are

$$\begin{aligned} S_1(\ell_1, \ell_2) &= 4g^2 \frac{(4\pi e^{\gamma_E} \mu^2)^\epsilon}{\Gamma(1-\epsilon)} C_F \int \frac{d^D k}{(2\pi)^D} \frac{1}{k^+ k^-} \mathcal{C}(k) \mathcal{M}_k^{(1)}(\ell_1, \ell_2) \\ &= \frac{\alpha_s(\mu) C_F}{\pi} \frac{(e^{\gamma_E} \mu^2)^\epsilon}{\Gamma(1-\epsilon)} \frac{1}{\epsilon} [\ell_1^{-1-2\epsilon} \delta(\ell_2) + \ell_2^{-1-2\epsilon} \delta(\ell_1)], \\ S_1(x_1, x_2) &= \frac{\alpha_s(\mu) C_F}{\pi} \frac{(e^{-\gamma_E})^\epsilon}{\Gamma(1-\epsilon)} \frac{\Gamma(-2\epsilon)}{\epsilon} [(ie^{\gamma_E} \mu x_1)^{2\epsilon} + (ie^{\gamma_E} \mu x_2)^{2\epsilon}]. \end{aligned} \quad (3.17)$$

At one-loop $Z_1(\ell_1, \ell_2, \mu) = Z_1(\ell_1, \mu) \delta(\ell_2) + \delta(\ell_1) Z_1(\ell_2, \mu)$ and $Z_1(x_1, x_2, \mu) = Z_1(x_1, \mu) + Z_1(x_2, \mu)$ and the momentum and position space counterterms are

$$\begin{aligned} Z_1(\ell_1, \mu) &= \frac{\alpha_s(\mu) C_F}{\pi} \left\{ -\frac{1}{2\epsilon^2} \delta(\ell_1) + \frac{1}{\epsilon} \frac{1}{\mu} \mathcal{L}_0\left(\frac{\ell_1}{\mu}\right) \right\}, \\ Z_1(x_1, \mu) &= \frac{\alpha_s(\mu) C_F}{\pi} \left\{ -\frac{1}{2\epsilon^2} - \frac{1}{\epsilon} \tilde{L}_1 \right\}, \end{aligned} \quad (3.18)$$

which will feed into the μ -dependent two-loop calculation. The remainder is the one-loop renormalized soft function in momentum and position space

$$\begin{aligned} S_1(\ell_1, \ell_2, \mu) &= \frac{\alpha_s(\mu) C_F}{\pi} \left\{ -\frac{2}{\mu} \mathcal{L}_1\left(\frac{\ell_1}{\mu}\right) \delta(\ell_2) - \frac{2}{\mu} \mathcal{L}_1\left(\frac{\ell_2}{\mu}\right) \delta(\ell_1) + \frac{\pi^2}{12} \delta(\ell_1) \delta(\ell_2) \right\}, \\ S_1(x_1, x_2, \mu) &= \frac{\alpha_s(\mu) C_F}{\pi} \left\{ -(\tilde{L}_1^2 + \tilde{L}_2^2) - \frac{\pi^2}{4} \right\}. \end{aligned} \quad (3.19)$$

| | | | | | |
|--------------|-------|----------|----------------------|----------|-------|
| | | | | | |
| Type: | V_2 | V_1Z_1 | V_1R_1 | Z_1R_1 | R_2 |
| Color: | all | C_F^2 | $\{C_F^2, C_F C_A\}$ | C_F^2 | all |
| x_1, x_2 : | none | single | single | both | both |

Table 1: Examples of various types of loop graphs which enter at $\mathcal{O}(\alpha_s^2)$ and their general properties. V_2 and R_2 are the $\mathcal{O}(\alpha_s^2)$ purely virtual and purely real graphs, V_1R_1 are the mixed virtual-real graphs, and Z_1 is the one-loop counterterm. For each class we indicate the color structures, and whether the graphs depend simultaneously on $x_{1,2}$ (in position space), on only a single variable at a time, or neither variable. The two-loop counterterm Z_2 is discussed in the text.

3.2 Structure of the $\mathcal{O}(\alpha_s^2)$ Real and Virtual Terms

The structure of the various types of $\mathcal{O}(\alpha_s^2)$ diagrams for the calculation of $\tilde{S}(x_1, x_2)$ are shown in Table 1. In dimensional regularization the bare two-loop virtual graphs and one-loop virtual graphs with a counterterm are scaleless and need not be considered. The remaining terms can all be divided into single hemisphere contributions that depend on a function of x_1 plus the same function of x_2 , and opposite hemisphere contributions that depend simultaneously on $x_{1,2}$ and contribute non-global terms. The bare and counterterm graphs can all be split into the form

$$\tilde{S}(x_1, x_2) = [\tilde{S}^{\text{same}}(x_1) + \tilde{S}^{\text{same}}(x_2)] + \tilde{S}^{\text{opp}}(x_1, x_2) \quad (3.20)$$

as follows. Consider the two-loop counterterm $Z_2(x_1, x_2, \mu)$, from Eq. (3.3)

$$Z_2(x_1, x_2, \mu) = Z_2(x_1, \mu) + Z_2(x_2, \mu) + Z_1(x_1, \mu)Z_1(x_2, \mu), \quad (3.21)$$

which is the appropriate form for Eq. (3.20), and shows that only Z_1 contributes to \tilde{S}^{opp} . Graphs that have only a single parton crossing the cut involve $\mathcal{M}_k^{[1]}(x_1, x_2)$ from Eq. (3.8) and are part of the single hemisphere terms. This includes the mixed virtual-real graphs denoted by V_1R_1 in Table 1. For the double cut real emission graphs the measurement function $\mathcal{M}_{k_1, k_2}^{[2]}(x_1, x_2)$ in Eq. (3.9) splits the result into a sum of single hemisphere and opposite hemisphere terms,

$$R_2(x_1, x_2) = [R_2^{\text{same}}(x_1) + R_2^{\text{same}}(x_2)] + R_2^{\text{opp}}(x_1, x_2), \quad (3.22)$$

where $R_2^{\text{same}}(x_1)$ involves $\mathcal{M}_{k_1, k_2}^{[LL]}(x_1, x_2)$, $R_2^{\text{same}}(x_2)$ involves $\mathcal{M}_{k_1, k_2}^{[RR]}(x_1, x_2)$, and $R_2^{\text{opp}}(x_1, x_2)$ involves $\mathcal{M}_{k_1, k_2}^{[LR]}(x_1, x_2)$. Using results from Sec. 3.1 the R_1Z_1 results can also be directly manipulated into the required form in Eq. (3.20).

Next consider the color structures of various opposite hemisphere contributions. From Eq. (3.21) and Table 1 we see that for $\tilde{S}^{\text{opp}}(x_1, x_2)$ both Z_2 and Z_1R_1 only contribute to C_F^2 . Hence these terms are just part of the exponentiation of the one-loop result, and are not needed for our computation of the unknown terms with color structures $C_F C_A$

and $C_F T_{Rn_f}$ which appear in $t_2(x_1/x_2)$ (see Sec. 2.2). Thus the only term we need to consider is the double cut real emission graphs R_2^{OPP} , and there are no UV divergences or counterterms for the color structures of interest in our calculation.

Before proceeding to analyze results of our computation of $R_2^{\text{OPP}}(x_1, x_2)$, we must address one important issue, namely that only the sum of \tilde{S}^{OPP} and \tilde{S}^{same} terms in Eq. (3.20) is infrared finite. From our computation discussed in Sec. 3.3 and Appendix B we find the infrared divergent terms in dimensional regularization are

$$R_2^{\text{OPP}}(x_1, x_2) = \frac{\alpha_s^2(\mu)}{(2\pi)^2} \left[C_F C_A \left(\frac{\pi^2}{6\epsilon^2} + \frac{11\pi^2 - 3}{18\epsilon} \right) + C_F T_{Rn_f} \frac{3 - 2\pi^2}{9\epsilon} \right] (ix_1 ix_2 \mu^2 e^{2\gamma_E})^{2\epsilon} + \dots \quad (3.23)$$

Here the ellipses denote IR finite terms and terms with the C_F^2 color structure. The divergences in Eq. (3.23) cancel against same hemisphere contributions, and hence determine the IR structure in \tilde{S}^{same} . In dimensional regularization the graphs contributing to $\tilde{S}^{\text{same}}(x_1, \mu)$ give powers of $(ix_1 \mu)^\epsilon$ determined by dimensional analysis and whether the graph involves counterterms, times functions of ϵ . Since the same hemisphere graphs involving Z_1 do not involve the color structures shown in Eq. (3.23), the IR divergent contributions which cancel those in Eq. (3.23) can only come from R_2^{same} and $V_1 R_1$. They are therefore uniquely determined to be

$$S_2^{\text{same}}(x_1, x_2) = \frac{-\alpha_s^2(\mu)}{(2\pi)^2} \left[C_F C_A \left(\frac{\pi^2}{6\epsilon^2} + \frac{11\pi^2 - 3}{18\epsilon} \right) + C_F T_{Rn_f} \frac{3 - 2\pi^2}{9\epsilon} \right] \times \frac{(ix_1 \mu e^{\gamma_E})^{4\epsilon} + (ix_2 \mu e^{\gamma_E})^{4\epsilon}}{2} + \dots \quad (3.24)$$

Adding and expanding Eqs. (3.23) and (3.24) the terms involving these IR divergences cancel, but leave a finite remainder

$$R_2^{\text{OPP}}(x_1, x_2) + S_2^{\text{same}}(x_1, x_2) = -\frac{\alpha_s^2(\mu)}{4\pi^2} C_F C_A \frac{\pi^2}{3} \ln^2 \left(\frac{x_1}{x_2} \right) + \dots \quad (3.25)$$

Thus the $1/\epsilon$ terms in $R_2^{\text{OPP}}(x_1, x_2)$ shown in Eq. (3.23) can be dropped if we replace them by the double logarithm in Eq. (3.25). The calculation of the opposite hemisphere infrared finite terms in the ellipses then proceeds without further complications.

Our result in Eq. (3.25) yields precisely the coefficient $s_2^{[2]} = -2\pi^2/3$ of the non-global logarithm discussed in Sec. 2.4 and first computed in Ref. [20]. The procedure discussed here to determine the non-global logarithm was first presented at the SCET 2011 workshop [45], including the fact that it can be computed by an effective theory that refactorizes scales in the soft function, and has ultraviolet divergences with the same coefficient as the above infrared divergences.

Accounting for the cancellation of IR divergences, the full renormalized soft function can be arranged into what we will refer to as renormalized same hemisphere contributions that depends on μ and one of the x variables, and a renormalized opposite hemisphere contribution that depends on x_1/x_2 ,

$$\tilde{S}_2(x_1, x_2, \mu) = [\tilde{S}_2^{\text{same}}(x_1, \mu) + \tilde{S}_2^{\text{same}}(x_2, \mu)] + \tilde{S}_2^{\text{OPP}}(x_1/x_2, \alpha_s(\mu)). \quad (3.26)$$

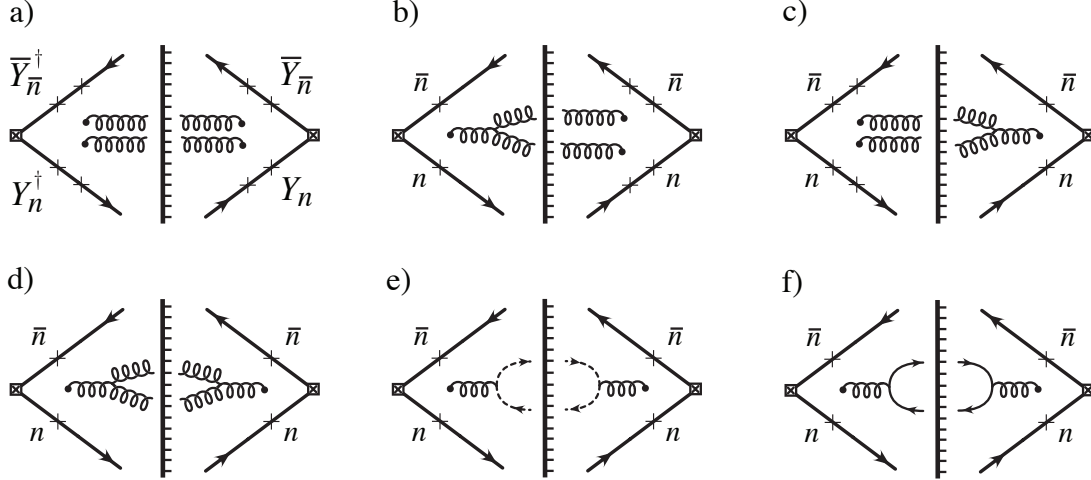


Figure 1: $\mathcal{O}(\alpha_s^2)$ opposite hemisphere diagrams. The endpoints of the gluons can be attached to the points on the Wilson lines labeled by a ‘x’ in any order. Figure (a) gives the \mathcal{I} diagrams, (b) and (c) give the \mathcal{T} diagrams, (d) gives the \mathcal{G} diagrams, (e) the \mathcal{H} diagrams with ghosts, and (f) the \mathcal{Q} diagrams with massless quarks.

Here the double log in Eq. (3.25) is included in $\tilde{S}_2^{\text{opp}}(x_1/x_2, \alpha_s(\mu))$. We present our full result for $\tilde{S}_2^{\text{opp}}(x_1/x_2, \alpha_s(\mu))$ in the next section. In dimensional regularization the graphs contributing to $\tilde{S}_2^{\text{same}}(x_1, \mu)$ give powers of $(ix_1\mu)^\epsilon$ times functions of ϵ , and hence only depend on the μ dependent logs L_1 in Eq. (3.15). At $\mathcal{O}(\alpha_s^2)$ the general result is

$$\tilde{S}_2^{\text{same}}(x_1, \mu) = a_4 \tilde{L}_1^4 + a_3 \tilde{L}_1^3 + a_2 \tilde{L}_1^2 + a_1 \tilde{L}_1 + a_0. \quad (3.27)$$

Since the logarithms from infrared divergences appear in S^{opp} all the \tilde{L}_1 terms in Eq. (3.27) are determined by the known anomalous dimensions for the soft function, through the RGE solution discussed in Sec. 2.2. Hence the only thing not determined by the above general considerations and our opposite hemisphere calculation of R_2 is the $C_F C_A$ and $C_F T_R n_f$ color factor terms in the constant a_0 . These two terms contribute directly to the two thrust constants $s_2^{[a]}$ in Eq. (2.17). We will present our final result as an analytic function of \tilde{L}_1 , \tilde{L}_2 , and $b = x_1/x_2$, plus $s_2^{[C_F C_A]}$ and $s_2^{[C_F n_f]}$ whose numerical values are given in Sec. 2.3.

3.3 Final Dijet Hemisphere Soft Functions

In Sec. 3.2 we showed that up to a constant the entire $\mathcal{O}(\alpha_s^2)$ dijet hemisphere soft function can be computed from the opposite hemisphere double real emission graphs and the known $\mathcal{O}(\alpha_s^2)$ anomalous dimensions. For this calculation there are five classes of diagrams shown in Fig. 1: independent emission (\mathcal{I}) diagrams, diagrams with a single three-gluon vertex (\mathcal{T}), and vacuum polarization diagrams with a gluon loop (\mathcal{G}), quark loop (\mathcal{Q}), or ghost loop (\mathcal{H}). Note that the C_F^2 color structure only appears in \mathcal{I} , and $C_F T_R n_f$ only appears in \mathcal{Q} , whereas the $C_F C_A$ color structure appears in all classes except \mathcal{Q} . For any graph

whose squared matrix element is \mathcal{A}_i , the opposite hemisphere contribution is

$$\int \frac{d^d k_1}{(2\pi)^d} \frac{d^d k_2}{(2\pi)^d} \mathcal{A}_i(k_1, k_2) \mathcal{M}_{k_1, k_2}^{[LR]} \mathcal{C}(k_1) \mathcal{C}(k_2), \quad (3.28)$$

where $\mathcal{C}(k)$ is the cut propagator, Eq. (3.5), $\mathcal{A}_i = \{\mathcal{I}, \mathcal{T}, \mathcal{G}, \mathcal{H}, \mathcal{Q}\}$ and the measurement function $\mathcal{M}_{k_1, k_2}^{[LR]}$ is given in Eq. (3.12) for both position space and momentum space. We present details of their calculation using Feynman gauge in both position and momentum space in Appendix B. The results appear in the following equations:

$$\begin{aligned} \mathcal{I} : & \text{Eqs.([B.26, B.32], [B.27 \& B.35])} , & \mathcal{T} : & \text{Eqs.(B.32, B.35)} , & \mathcal{G} : & \text{Eqs.(B.40, B.43)} , \\ \mathcal{H} : & \text{Eqs.(B.40, B.43)} , & \mathcal{Q} : & \text{Eqs.(B.47, B.50)} . \end{aligned} \quad (3.29)$$

We have explicitly checked that our final result is unchanged if the gluon propagators in Fig. 1 are taken in a general covariant gauge. The gauge parameter cancellation occurs individually for the \mathcal{T} , $\mathcal{G} + \mathcal{H}$, and \mathcal{Q} terms (and provides a non-trivial cross check on the relative overall signs of \mathcal{G} and \mathcal{H}).

Next we present final results for the renormalized soft function that includes contributions from both the same hemisphere and opposite hemisphere terms, using the approach described in Sec. 3.2. We first discuss position space and then the double cumulant distribution in momentum space. Eqs. (3.30) and (3.35) are the main results of this paper.

3.3.1 Result in Position Space

In position space we find

$$\begin{aligned} S(x_1, x_2, \mu) = & 1 - \frac{\alpha_s(\mu) C_F}{4\pi} \pi^2 + \tilde{R}(x_1, x_2, \mu) + \frac{\alpha_s^2(\mu)}{4\pi^2} \left\{ -C_F C_A \frac{\pi^2}{3} \ln^2 \left(\frac{x_1}{x_2} \right) \right. \\ & + \ln \left(\frac{x_1/x_2 + x_2/x_1}{2} \right) \left[C_F C_A \frac{(11\pi^2 - 3 - 18\zeta_3)}{9} + C_F T_R n_f \left(\frac{6 - 4\pi^2}{9} \right) \right] \\ & + C_F T_R n_f \left[F_Q \left(\frac{x_1}{x_2} \right) + F_Q \left(\frac{x_2}{x_1} \right) - 2F_Q(1) \right] + C_F C_A \left[F_N \left(\frac{x_1}{x_2} \right) + F_N \left(\frac{x_2}{x_1} \right) - 2F_N(1) \right] \\ & \left. + C_F^2 \frac{\pi^4}{8} + \frac{1}{2} C_F C_A s_2^{[C_F C_A]} + \frac{1}{2} C_F T_R n_f s_2^{[n_f]} \right\}, \end{aligned} \quad (3.30)$$

where here and throughout this paper x_1 and x_2 have a small imaginary components, and should be regarded as $x_1 - i0^+$ and $x_2 - i0^+$. Values for the $s_2^{[a]}$ coefficients are given in Sec. 2.3, the functions are

$$\begin{aligned} F_Q(b) &= \frac{2 \ln b}{3(b-1)} - \frac{b \ln^2 b}{3(b-1)^2} - \frac{(3-2\pi^2)}{9} \ln \left(b + \frac{1}{b} \right) + \frac{2}{3} \ln^2 b \ln(1-b) + \frac{8}{3} \ln b \text{Li}_2(b) - 4 \text{Li}_3(b), \\ F_N(b) &= -\frac{\pi^4}{36} - \frac{\ln b}{3(b-1)} + \frac{b \ln^2 b}{6(b-1)^2} + \frac{(3-11\pi^2+18\zeta_3)}{18} \ln \left(b + \frac{1}{b} \right) - \frac{11}{6} \ln^2 b \ln(1-b) + \frac{\ln^4 b}{24} \\ & \quad - \frac{\pi^2}{3} \text{Li}_2(1-b) + [\text{Li}_2(1-b)]^2 - \frac{22}{3} \ln b \text{Li}_2(b) + 2 \ln b \text{Li}_3(1-b) + 11 \text{Li}_3(b), \end{aligned} \quad (3.31)$$

and the formula for the μ -dependent terms, $\tilde{R}(x_1, x_2, \mu)$, will be given below. The result in Eq. (3.30) is written so that the double and single logarithmic singularities for $b = x_1/x_2 \rightarrow$

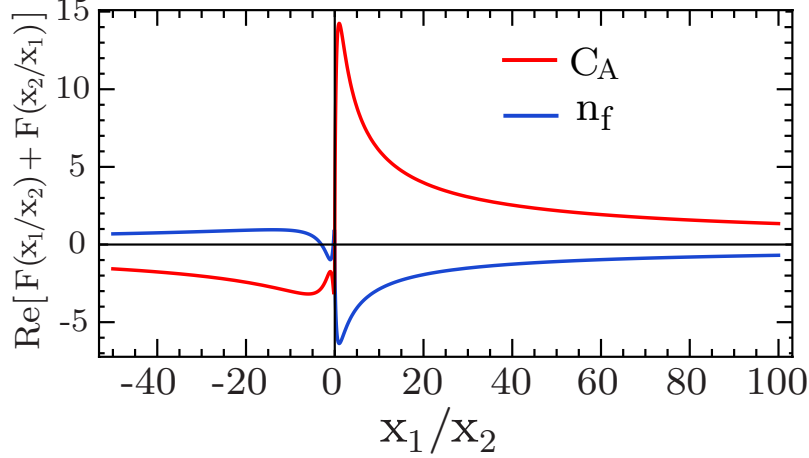


Figure 2: The non-logarithmic non-global function in position space. We show the functions $\text{Re}[F(b) + F(1/b)]$, where $b = x_1/x_2$, that appear in the position-space soft function Eq. (3.30) for the color structures C_{FC_A} (solid red) and $C_{FT_R n_f}$ (solid blue).

0 and $b \rightarrow \infty$ are separated out in the first two lines. The more complicated structures in $F_Q(b) + F_Q(1/b)$ and $F_N(b) + F_N(1/b)$ are bounded functions whose real parts go to zero for $b \rightarrow 0$ and $b \rightarrow \infty$. For negative $\text{Re} b$, the functions also have an imaginary part. The real parts are illustrated in Fig. 2. The final result for $t_2(x_1/x_2)/2$ appearing in Eq. (2.13) is given by all the terms in the $\{\dots\}$ in Eq. (3.30), except for the one term determined by exponentiation that involves C_F^2 .

Taking the $x_1 \gg x_2$ limit discussed in Eq. (2.24) yields terms $s_2^{[i]} \ln^i(x_1/x_2)$ at $\mathcal{O}(\alpha_s^2)$ and our result in Eq. (3.30) determines the coefficients

$$s_2^{[2]} = -\frac{2\pi^2}{3} C_{FC_A}, \quad s_2^{[1]} = -2 \left[C_{FC_A} \frac{(11\pi^2 - 3 - 18\zeta_3)}{9} + C_{FT_R n_f} \left(\frac{6 - 4\pi^2}{9} \right) \right], \quad (3.32)$$

$$s_2^{[0]} = -s_2^{[1]} \ln 2 - C_{FC_A} 2F_N(1) - C_{FT_R n_f} 2F_Q(1) + C_F^2 \frac{\pi^4}{4} + C_{FC_A} s_2^{[C_{FC_A}]} + C_{FT_R n_f} s_2^{[n_f]},$$

where

$$2F_Q(1) = \frac{2}{3} + \left(\frac{4\pi^2}{9} - \frac{2}{3} \right) \ln 2 - 8\zeta_3, \quad (3.33a)$$

$$2F_N(1) = -\frac{1}{3} - \frac{\pi^4}{18} + \left(\frac{1}{3} - \frac{11\pi^2}{9} + 2\zeta_3 \right) \ln 2 + 22\zeta_3. \quad (3.33b)$$

In the left panel of Fig. 3 we plot the double log (dotted), single log (dashed), and non-log (solid) $\mathcal{O}(\alpha_s^2)$ non-global contributions to $\tilde{S}(x_1, x_2, \mu)$ as a function of x_1/x_2 . Results are shown separately for the C_{FC_A} and $C_{FT_R n_f}$ color structures with overall signs for the plot chosen so that the former are negative and latter positive, which involves plotting the single NGL terms $\propto \ln(b + 1/b)$ with the opposite sign. The solid lines are the non-logarithmic functions $[F_{N,Q}(b) + F_{N,Q}(1/b) - 2F_{N,Q}(1) + \frac{1}{2}s_2^{[C_{FC_A}, n_f]}]$, the dashed lines are the single NGL terms, and the dotted black line is the double NGL $\propto \ln^2 b$ (nonzero only for C_{FC_A}), where $b = x_1/x_2$. For values in the vicinity of $x_1 = x_2$ the contributions from all sources

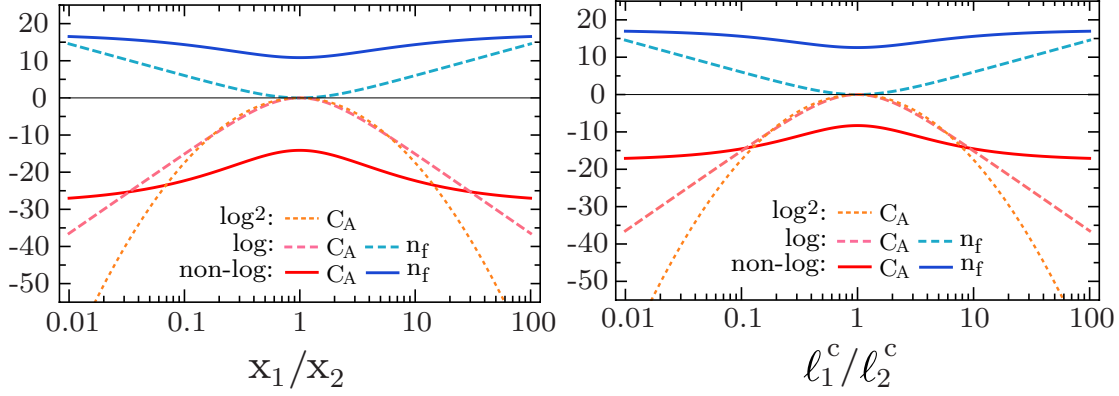


Figure 3: Non-global logarithms and non-global non-logarithms in position space as a function of x_1/x_2 (left panel) and in cumulant momentum space as a function of ℓ_1^c/ℓ_2^c (right panel). We plot separately the \log^2 (dotted), \log (dashed), and non-log (solid) parts of the various functions that appear in the soft functions $\tilde{S}(x_1, x_2, \mu)$ and $\mathcal{S}_c(\ell_1^c, \ell_2^c, \mu)$ (ignoring the μ dependent terms in \tilde{R} and \mathcal{R}_c). The single log curves have been plotted with the opposite sign.

are comparable in size and the non-analytic non-log dependences are important. As we already remarked, the F dependent terms exhibit a smooth bounded behavior.

Expanding Eq. (2.12) and inserting the known anomalous dimensions the $\tilde{L}_{1,2} = \ln(ix_{1,2}e^{\gamma_E}\mu)$ dependent part of the soft function, $\tilde{R}(x_1, x_2, \mu)$, is

$$\begin{aligned}
\tilde{R}(x_1, x_2, \mu) = & -\frac{\alpha_s(\mu)C_F}{\pi} (\tilde{L}_1^2 + \tilde{L}_2^2) + \frac{\alpha_s^2(\mu)}{16\pi^2} \left\{ C_F^2 (8\tilde{L}_1^4 + 8\tilde{L}_2^4 + 16\tilde{L}_1^2\tilde{L}_2^2) \right. \\
& + \left(-\frac{88}{9}C_FC_A + \frac{32}{9}C_FT_Rn_f \right) (\tilde{L}_1^3 + \tilde{L}_2^3) \\
& + \left[4\pi^2C_F^2 - 4C_FC_A \left(\frac{67}{9} - \frac{\pi^2}{3} \right) + \frac{80}{9}C_FT_Rn_f \right] (\tilde{L}_1^2 + \tilde{L}_2^2) \\
& \left. + \left[C_FC_A \left(-\frac{808}{27} - \frac{22\pi^2}{9} + 28\zeta_3 \right) + C_FT_Rn_f \left(\frac{224}{27} + \frac{8}{9}\pi^2 \right) \right] (\tilde{L}_1 + \tilde{L}_2) \right\}. \quad (3.34)
\end{aligned}$$

3.3.2 Result in Momentum Space

Our complete result for the bare two-loop opposite hemisphere piece of the momentum space soft function $S(\ell_1, \ell_2)$ is given in Eq. (B.55). In Sec. 4.1 we describe how this result can be used to obtain the double cumulant $\mathcal{S}_c(\ell_1^c, \ell_2^c, \mu)$. The final result for the renormalized momentum space double cumulant distribution is

$$\begin{aligned}
\mathcal{S}_c(\ell_1^c, \ell_2^c, \mu) = & \theta(\ell_1^c)\theta(\ell_2^c) \left[1 - \frac{\alpha_s(\mu)C_F}{4\pi}\pi^2 + \mathcal{R}_c(\ell_1^c, \ell_2^c, \mu) + \frac{\alpha_s(\mu)^2}{4\pi^2} \left\{ -\frac{\pi^2}{3}C_FC_A \ln^2 \left(\frac{\ell_1^c}{\ell_2^c} \right) \right. \right. \\
& + \left[C_FC_A \frac{11\pi^2 - 3 - 18\zeta_3}{9} + C_FT_Rn_f \frac{6 - 4\pi^2}{9} \right] \ln \left(\frac{\ell_1^c/\ell_2^c + \ell_2^c/\ell_1^c}{2} \right) \\
& \left. \left. + C_FC_A \left[f_N \left(\frac{\ell_1^c}{\ell_2^c} \right) + f_N \left(\frac{\ell_2^c}{\ell_1^c} \right) - 2f_N(1) \right] + C_FT_Rn_f \left[f_Q \left(\frac{\ell_1^c}{\ell_2^c} \right) + f_Q \left(\frac{\ell_2^c}{\ell_1^c} \right) - 2f_Q(1) \right] \right\} \right]
\end{aligned}$$

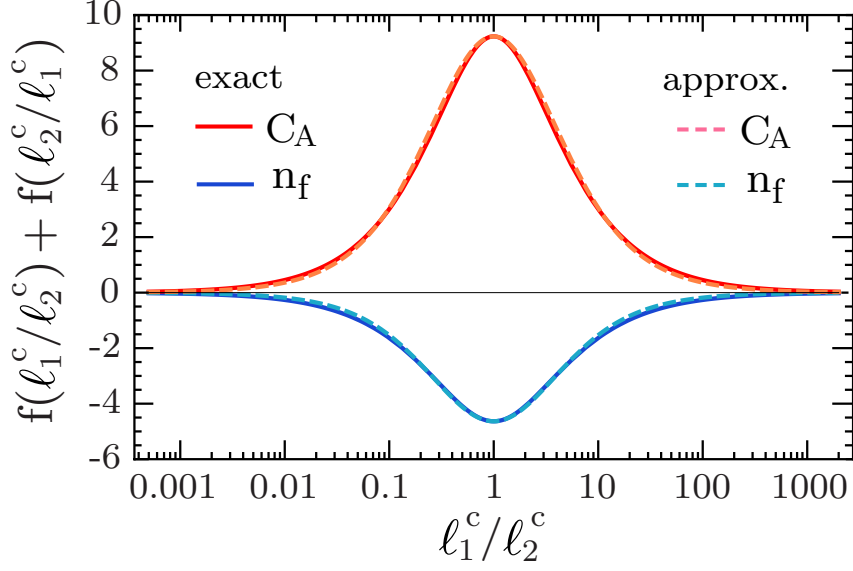


Figure 4: The non-logarithmic non-global function in momentum space. We show the functions $f(a) + f(1/a)$, where $a = \ell_1^c/\ell_2^c$, that appear in the momentum-space double cumulant Eq. (3.35) for the color structures $C_F C_A$ (solid red) and $C_F T_R n_f$ (solid blue). The simple approximate forms Eq. (3.39) of these functions are the dotted lines.

$$+ C_F^2 \frac{\pi^4}{8} + \frac{1}{2} C_F C_A s_{2\rho}^{[C_F C_A]} + \frac{1}{2} C_F T_R n_f s_{2\rho}^{[n_f]} \left. \right\} \Bigg], \quad (3.35)$$

where the logarithmic dependence is isolated on the first two lines and the remainder depends on the constants $s_{2\rho}^{[C_F C_A, n_f]}$, μ -dependent terms $\mathcal{R}_c(\ell_1^c, \ell_2^c, \mu)$ to be discussed below, and the functions

$$\begin{aligned} f_Q(a) &\equiv \left(\frac{2\pi^2}{9} - \frac{2}{3(a+1)} \right) \ln(a) - \frac{4}{3} \ln(a) \text{Li}_2(-a) + 4 \text{Li}_3(-a) - \frac{1}{9} (3 - 2\pi^2) \ln \left(a + \frac{1}{a} \right), \\ f_N(a) &\equiv -4 \text{Li}_4 \left(\frac{1}{a+1} \right) - 11 \text{Li}_3(-a) + 2 \text{Li}_3 \left(\frac{1}{a+1} \right) \ln \left[\frac{a}{(a+1)^2} \right] \\ &\quad + \text{Li}_2 \left(\frac{1}{a+1} \right) \left\{ \pi^2 - \ln^2(a+1) - \frac{1}{2} \ln(a) \ln \left[\frac{a}{(a+1)^2} \right] + \frac{11}{3} \ln(a) \right\} \\ &\quad + \frac{1}{24} \left\{ 22 \ln \left[\frac{a}{(a+1)^2} \right] - 6 \ln \left(1 + \frac{1}{a} \right) \ln(1+a) + \pi^2 \right\} \ln^2(a) - \frac{(a-1) \ln(a)}{6(a+1)} \\ &\quad + \frac{5\pi^2}{12} \ln \left(1 + \frac{1}{a} \right) \ln(1+a) - \frac{11\pi^4}{180} - \frac{(11\pi^2 - 3 - 18\zeta_3)}{18} \ln \left(a + \frac{1}{a} \right). \end{aligned} \quad (3.36)$$

The combinations $f_Q(a) + f_Q(1/a)$ and $f_N(a) + f_N(1/a)$ appearing in Eq. (3.35) are bounded functions of a , vanishing as $a \rightarrow 0$ or $a \rightarrow \infty$.

Taking the $\ell_1^c \gg \ell_2^c$ limit of Eq. (3.35) we see that the non-global logs in momentum space have the same coefficients as those in position space. We find

$$\frac{\alpha_s^2}{8\pi^2} \left[s_{2c}^{[2]} \ln^2 \left(\frac{\ell_1^c}{\ell_2^c} \right) + s_{2c}^{[1]} \ln \left(\frac{\ell_1^c}{\ell_2^c} \right) + s_{2c}^{[0]} + \dots \right], \quad (3.37)$$

where $s_{2c}^{[2]} = s_2^{[2]}$ and $s_{2c}^{[1]} = s_2^{[1]}$ from Eq. (3.32). The coefficient $s_{2c}^{[0]}$ is the same as $s_2^{[0]}$ in Eq. (3.32) except with the replacements $s_2^{[1]} \rightarrow s_{2c}^{[1]}$, $s_2^{[C_F C_A, n_f]} \rightarrow s_{2\rho}^{[C_F C_A, n_f]}$, and $F_N(1) \rightarrow f_N(1)$, $F_Q(1) \rightarrow f_Q(1)$. Here

$$2f_Q(1) = -6\zeta_3 - \frac{2}{9}(3 - 2\pi^2) \ln 2, \quad (3.38)$$

$$2f_N(1) = -8\text{Li}_4\left(\frac{1}{2}\right) + \zeta_3\left(\frac{33}{2} - 5 \ln 2\right) + \frac{\ln 2 - \ln^4 2}{3} + \frac{2\pi^4}{45} + \frac{\pi^2}{3}\left(\ln^2 2 - \frac{11}{3} \ln 2\right).$$

In the right panel of Fig. 3 we plot the double log (dotted), single log (dashed), and non-log (solid) non-global contributions to $\mathcal{S}_c(\ell_1^c, \ell_2^c, \mu)$. The overall signs for the plot are chosen so that the $C_F C_A$ color structures are negative and $C_F T_R n_f$ are positive, which involves plotting the single NGL $\propto \ln(a + 1/a)$, where $a = \ell_1^c / \ell_2^c$, with the opposite sign. The solid lines are the non-logarithmic functions $[f_{N,Q}(a) + f_{N,Q}(1/a) - 2f_{N,Q}(1) + \frac{1}{2}s_{2\rho}^{[C_F C_A, n_f]}]$ where $a = \ell_1^c / \ell_2^c$. Comparing to the left and right panels of Fig. 3 the log terms are identical, but the non-log terms differ.

The complicated functions in Eq. (3.36) are well approximated for all a by a simple function, taking the form

$$f_{Q,N}(a) + f_{Q,N}(1/a) \simeq 2f_{Q,N}(1) \frac{4a}{(1+a)^2}. \quad (3.39)$$

The comparison between the exact forms in Eq. (3.36) and the approximate forms in Eq. (3.39) is shown in Fig. Fig. 4.

The constant terms $s_{2\rho}^{[C_F C_A]}$ and $s_{2\rho}^{[n_f]}$ in Eq. (3.35) are given by the thrust constants $s_2^{[C_F C_A]}$ and $s_2^{[n_f]}$, plus analytic constants. In Sec. 4.3.2 we calculate the differences $s_{2\rho}^{[a]} - s_2^{[a]}$ analytically, and find

$$s_{2\rho}^{[n_f]} = s_2^{[n_f]} + 4\zeta_3 - \frac{4}{3}, \quad (3.40)$$

$$s_{2\rho}^{[C_F C_A]} = s_2^{[C_F C_A]} + \frac{2}{3} + \frac{19\pi^4}{45} + \frac{2\pi^2}{3} \ln^2 2 - \frac{2}{3} \ln^4 2 - 16\text{Li}_4\left(\frac{1}{2}\right) - 11\zeta_3 - 14\zeta_3 \ln 2.$$

Thus only the constants $s_2^{[C_F C_A, n_f]}$ remain in both of our final results Eqs. (3.30) and (3.35), and for them we use the numerical values quoted in Eq. (2.19) from Ref. [37].

The $\ln(\ell_1^c / \mu)$ and $\ln(\ell_2^c / \mu)$ dependent part $\mathcal{R}_\Sigma(\ell_1^c, \ell_2^c, \mu)$, obtainable by taking the inverse Fourier transform of Eq. (3.34), is given by

$$\begin{aligned} \mathcal{R}_c(\ell_1^c, \ell_2^c, \mu) = & -\frac{\alpha_s(\mu) C_F}{\pi} (L_1^2 + L_2^2) + \frac{\alpha_s^2(\mu)}{(4\pi)^2} \left\{ 8C_F^2 (L_1^4 + L_2^4) + 16C_F^2 L_1^2 L_2^2 + \left(\frac{88}{9}\right) C_F C_A \right. \\ & - \frac{32}{9} C_F T_R n_f \left. \right\} (L_1^3 + L_2^3) + \left[-\frac{20\pi^2}{3} C_F^2 + C_F C_A \left(\frac{4\pi^2}{3} - \frac{268}{9}\right) + \frac{80}{9} C_F T_R n_f \right] (L_1^2 + L_2^2) \\ & + \left[64\zeta_3 C_F^2 + C_F C_A \left(\frac{808}{27} - \frac{22\pi^2}{9} - 28\zeta_3\right) - C_F T_R n_f \left(\frac{224}{27} - \frac{8\pi^2}{9}\right) \right] (L_1 + L_2) \left. \right\}, \end{aligned} \quad (3.41)$$

where $L_1^n = \ln^n(\ell_1^c / \mu)$, and $L_2^n = \ln^n(\ell_2^c / \mu)$. Eq. (3.35) will be used in the double cumulant comparison to EVENT2 data done in Sec. 5.

4. Projection onto Other Observables

Having obtained the explicit analytic result for the dijet soft function, we can make use of it in several ways. In Sec. 4.1 we give further details about the projection of the momentum space result used to obtain the renormalized double cumulant, $\mathcal{S}_c(\ell_1^c, \ell_2^c, \mu)$ in Eq. (3.35), since the procedure is useful for other projections. Additionally, in Sec. 4.2 we project the distribution onto two classes of event shape observables, asymmetric thrust and asymmetric heavy jet mass, originally defined in [21]. Asymmetric thrust can be defined from the hemisphere masses m_1^2 and m_2^2 as

$$\tau_\alpha = \frac{2}{1+\alpha} \frac{\alpha m_1^2 + m_2^2}{Q^2}, \quad (4.1)$$

where $\alpha > 0$ is a dimensionless parameter. In the dijet limit τ_α corresponds to the original thrust for $\alpha = 1$. The asymmetric heavy jet mass is

$$\rho_\alpha = \frac{2}{1+\alpha} \max\left(\alpha \frac{m_1^2}{Q^2}, \frac{m_2^2}{Q^2}\right), \quad (4.2)$$

and corresponds to the heavy-jet-mass for $\alpha = 1$. The $d\sigma/d\tau_\alpha$ and $d\sigma/d\rho_\alpha$ distributions contain non-global logarithms in α , and we will show that the full non-global structure of their cumulants bears close relation to the non-global structure in the position space dijet cross section and the double cumulant momentum space cross-section.

As discussed in Sec. 2.3, the projection of the non-global structure onto the two loop terms needed for the heavy jet mass and thrust is of interest. These observables have recently been used in fits of α_s from e^+e^- collider data, placing importance on the knowledge of these constants [16, 22, 46, 18]. In Sec. 4.3 we project our non-global results onto heavy jet mass and thrust and determine the difference between the cumulants of the heavy jet mass and thrust distributions, Eq. (2.22), from the dijet hemisphere mass distribution. We compare our analytic result, Eq. (4.28), to a numerical projection from our position space result and to a numerical extraction from EVENT2, Eq. (2.23), both of which provide a nontrivial cross-check of our calculations.

4.1 The Double Cumulant of the Non Global Terms

To determine the double cumulant of the non-global terms, we compute the opposite hemisphere cumulant

$$\mathcal{S}_c^{\text{opp}}(\ell_1^c, \ell_2^c) = \int^{\ell_1^c} dl_1 \int^{\ell_2^c} dl_2 S^{\text{opp}}(\ell_1, \ell_2), \quad (4.3)$$

The function $S^{\text{opp}}(\ell_1, \ell_2)$ only has support for $\ell_1, \ell_2 \geq 0$. The relation of this double cumulant soft function to the position space soft function is

$$\mathcal{S}_c^{\text{opp}}(\ell_1^c, \ell_2^c) = - \int \frac{dx_1}{2\pi} \frac{dx_2}{2\pi} \exp(i\ell_1^c x_1 + i\ell_2^c x_2) \frac{\tilde{S}(x_1, x_2)}{(x_1 x_2)}, \quad (4.4)$$

where $x_i \equiv x_i - i0^+$ in the above equation. Comparing this result to Eq. (4.13) with $\alpha = 1$ we see that the diagonal projection $S^{\text{opp}}(\ell_1^c, \ell_1^c)$ is equal to the heavy jet mass cumulant

with $\ell_1^c = Q\rho_H$, which explains the appearance of the heavy jet mass constants $s_{2\rho}^{[C_F C_A, n_f]}$ in our final result in Eq. (3.35).

For the analytic computation of the dependence on ℓ_1^c/ℓ_2^c from the opposite hemisphere terms it is more convenient to start with the bare momentum space result. We use the general form of the opposite hemisphere results from Eq. (B.13):

$$S^{\text{opp}[i]}(\ell_1, \ell_2, \mu) = A C_i \mu^{4\epsilon} s^{-1-2\epsilon} [F_0 + F_1(r)], \quad (4.5)$$

where the variables

$$s = \ell_1 \ell_2, \quad r = \frac{\ell_1}{\ell_2}, \quad (4.6)$$

the color factor $C_i = C_F C_A$ or $C_F T_R n_f$, F_0 and $F_1(r)$ depend on the class of diagram (see Fig. 1) contributing to $S_{\text{opp}}^{[i]}$ and with μ in $\overline{\text{MS}}$ the prefactor

$$A = \left(\frac{\alpha_s}{2\pi}\right)^2 \frac{(e^{\gamma_E})^{2\epsilon}}{\Gamma(1-\epsilon)^2} = \left(\frac{\alpha_s}{2\pi}\right)^2 \left(1 - \frac{\pi^2}{6}\epsilon^2 + \mathcal{O}(\epsilon^3)\right). \quad (4.7)$$

To evaluate the double cumulant we change variables to s and r :

$$\mathcal{S}_c^{\text{opp}}(\ell_1^c, \ell_2^c) = \int_0^{\ell_1^c/\ell_2^c} \frac{dr}{2r} \int_0^{(\ell_2^c)^2 r} ds S^{\text{opp}}(\ell_1, \ell_2) + \int_{\ell_1^c/\ell_2^c}^\infty \frac{dr}{2r} \int_0^{(\ell_1^c)^2/r} ds S^{\text{opp}}(\ell_1, \ell_2). \quad (4.8)$$

Plugging in the form in Eq. (4.5), we can perform the s integral. Then expanding to collect terms, we find

$$\begin{aligned} \mathcal{S}_c^{\text{opp}[i]}(\ell_1^c, \ell_2^c) = C_i \left\{ \frac{1}{4\epsilon^2} A \left(\frac{\mu^2}{\ell_1^c \ell_2^c}\right)^{2\epsilon} - \left(\frac{\alpha_s}{2\pi}\right)^2 \frac{1}{4\epsilon} \left(\frac{\mu^2}{\ell_1^c \ell_2^c}\right)^{2\epsilon} \int_0^\infty \frac{dr}{r} F_1(r) \right. \\ \left. + \frac{1}{2} \left(\frac{\alpha_s}{2\pi}\right)^2 \int_0^{\ell_1^c/\ell_2^c} \frac{dr}{r} \ln\left(r \frac{\ell_2^c}{\ell_1^c}\right) F_1(r) + \frac{1}{2} \left(\frac{\alpha_s}{2\pi}\right)^2 \int_0^{\ell_2^c/\ell_1^c} \frac{dr}{r} \ln\left(r \frac{\ell_1^c}{\ell_2^c}\right) F_1(r) \right\}. \end{aligned} \quad (4.9)$$

The final two terms contain only finite μ -independent terms which contribute to \mathcal{S} . The first two terms contain μ -dependent terms, some of which cancel with the same hemisphere terms. The only term that does not cancel, but combines in a non-trivial way, is the double logarithmic term. Putting these terms together, the cumulant of the non-global terms \mathcal{S} is

$$\begin{aligned} \mathcal{S}_c^{\text{opp}[i]}(\ell_1^c, \ell_2^c) = \left(\frac{\alpha_s}{2\pi}\right)^2 C_i \left\{ -\frac{1}{2} F_0 \ln^2\left(\frac{\ell_1^c}{\ell_2^c}\right) \right. \\ \left. + \frac{1}{2} \int_0^{\ell_1^c/\ell_2^c} \frac{dr}{r} \ln\left(r \frac{\ell_2^c}{\ell_1^c}\right) F_1(r) + \frac{1}{2} \int_0^{\ell_2^c/\ell_1^c} \frac{dr}{r} \ln\left(r \frac{\ell_1^c}{\ell_2^c}\right) F_1(r) + \mathcal{S}_0 \right\}, \end{aligned} \quad (4.10)$$

where in F_0 and $F_1(r)$ we only keep the $\mathcal{O}(\epsilon^0)$ terms. \mathcal{S}_0 is the constant term in the non-global terms. Note that our calculation of $\mathcal{S}_c^{\text{opp}[C_F C_A]}$ has

$$F_0 = \frac{2\pi^2}{3} + \mathcal{O}(\epsilon). \quad (4.11)$$

We can perform these integrals analytically for the total momentum space result from all graphs, given by Eq. (B.55). The final result for the double cumulant with both opposite and same hemisphere terms is given above in Eq. (3.35).

4.2 Asymmetric Heavy Jet Mass and Asymmetric Thrust

In this section we give the projection from both the position and momentum space opposite hemisphere terms onto asymmetric heavy jet mass and asymmetric thrust. We will use the $\alpha = 1$ results of these projections to extract the difference in the constant terms of heavy jet mass and thrust. Projecting both forms of hemisphere soft function result, position and momentum space, onto the asymmetric heavy jet mass and asymmetric thrust cumulants provides a nontrivial check of the consistency of our results and uncovers interesting relations for the hemisphere soft function. We present the relevant projections starting from the hemisphere soft function in both spaces.

The asymmetric thrust cumulant is defined from the momentum space and position space hemisphere mass soft function by the projections [21]

$$\begin{aligned}\Sigma_{\tau_\alpha}(\tau_\alpha^c) &= \int_0^{\tau_\alpha^c} d\tau_\alpha \int dm_1^2 dm_2^2 \delta\left(\tau_\alpha - \frac{2}{1+\alpha} \frac{\alpha m_1^2 + m_2^2}{Q^2}\right) \frac{d^2\sigma}{dm_1^2 dm_2^2}, \\ \Sigma_{\tau_\alpha}(\tau_\alpha^c) &= -i \int \frac{dy}{2\pi} \exp(iQ^2 \tau_\alpha y) \frac{\tilde{\sigma}(\alpha y, y)}{y - i0^+}.\end{aligned}\quad (4.12)$$

Similarly, the asymmetric heavy jet mass distribution is defined from the momentum space and position space hemisphere mass distributions by [21]

$$\begin{aligned}\Sigma_{\rho_\alpha}(\rho_\alpha^c) &= \int_0^{\rho_\alpha^c} d\rho_\alpha \int dm_1^2 dm_2^2 \delta\left(\rho_\alpha - \frac{2}{1+\alpha} \frac{\max(\alpha m_1^2, m_2^2)}{Q^2}\right) \frac{d^2\sigma}{dm_1^2 dm_2^2}, \\ \Sigma_{\rho_\alpha}(\rho_\alpha^c) &= - \int \frac{dy_1}{2\pi} \frac{dy_2}{2\pi} \exp(iQ^2 \rho_\alpha (y_1 + y_2)) \frac{\tilde{\sigma}(\alpha y_1, y_2)}{(y_1 - i0^+)(y_2 - i0^+)}.\end{aligned}\quad (4.13)$$

4.2.1 Projection for the Non-Global Terms from Position Space

Lets consider the contribution to the two asymmetric event shapes from the non-global term. In position space we can determine this contribution by inserting $\tilde{\sigma}(y_1, y_2) = \alpha_s^2/(8\pi^2)t_2(y_1/y_2)$ into Eqs. (4.12) and (4.13).

For asymmetric thrust this gives

$$\begin{aligned}\Sigma_{\tau_\alpha}^{[t_2]}(\tau_\alpha^c) &= \left(\frac{\alpha_s^2}{8\pi^2}\right)(-i) \int \frac{dy}{2\pi} \exp(iQ^2 \tau_\alpha y) \frac{t_2(\alpha)}{y - i0^+} \\ &= \left[\frac{\alpha_s^2}{8\pi^2} t_2(\alpha)\right] \theta(\tau_\alpha^c).\end{aligned}\quad (4.14)$$

This result tells us that the non-global dependence on α of asymmetric thrust, given by $t_2(\alpha)$, is equivalent to the non-global dependence on x_1/x_2 in the position space hemisphere soft function, given by $t_2(x_1/x_2)$. We will see a similar correspondence for asymmetric heavy jet mass in the momentum space projection.

For asymmetric heavy jet mass the fact that t_2 only depends on the ratio of positions motivates making the following change of variables in Eq. (4.13):

$$i\theta = \ln \frac{y_1 - i0^+}{y_2 - i0^+}, \quad z = y_1 + y_2 - i0^+ \quad \implies \quad \frac{id\theta dz}{(z - i0^+)} = \frac{dy_1 dy_2}{(y_1 - i0^+)(y_2 - i0^+)}. \quad (4.15)$$

This gives

$$\begin{aligned}\Sigma_{\rho_\alpha}^{[t_2]}(\rho_\alpha^c) &= \frac{\alpha_s^2}{8\pi^2} \int \frac{d\theta}{2\pi} \frac{dz}{2\pi} \frac{(-i)}{z-i0^+} \exp(iQ^2\rho_\alpha^c z) t_2(\alpha e^{i\theta}) \\ &= \left[\frac{\alpha_s^2}{8\pi^2} \int_0^\pi \frac{d\theta}{\pi} t_2(\alpha e^{i\theta}) \right] \theta(\rho_\alpha^c).\end{aligned}\quad (4.16)$$

The projection again just gives a θ -function, but this time a more complicated projection from t_2 is needed to get the coefficient.

Note that the calculation used to obtain Eqs. (4.14) and (4.16) is also valid for cross-section terms appearing at higher orders in α_s as long as they are only functions of x_1/x_2 .

4.2.2 Projection from Momentum Space

For both asymmetric heavy jet mass and asymmetric thrust, we consider the projection for the bare opposite hemisphere terms and remove the μ -dependent pieces to obtain the projection for the non-global terms. To perform the projection, we change variables from ℓ_1, ℓ_2 to s and r in Eq. (4.6). For asymmetric heavy jet mass, the cumulant for the opposite hemisphere terms is

$$\mathcal{S}_{c\rho_\alpha}^{\text{opp}}(\rho_\alpha^c) = \int_0^\rho d\rho_\alpha \int d\ell_1 d\ell_2 \delta\left(\rho_\alpha - \frac{2}{1+\alpha} \max\left(\alpha \frac{\ell_1}{Q}, \frac{\ell_2}{Q}\right)\right) S^{\text{opp}}(\ell_1, \ell_2, \mu). \quad (4.17)$$

Using the general form in Eq. (4.5), the cumulant in terms of integrals over s and r is

$$\begin{aligned}\mathcal{S}_{c\rho_\alpha}^{\text{opp}[i]}(\rho_\alpha^c) &= \int_0^{1/\alpha} \frac{dr}{2r} \int_0^{r\rho^2((1+\alpha)/2)^2} ds A C_i \mu^{4\epsilon} s^{-1-2\epsilon} (F_0 + F_1(r)) \\ &\quad + \int_{1/\alpha}^\infty \frac{dr}{2r} \int_0^{\frac{1}{r}\rho^2((1+\alpha)/2\alpha)^2} ds A C_i \mu^{4\epsilon} s^{-1-2\epsilon} (F_0 + F_1(r)).\end{aligned}\quad (4.18)$$

Performing the s integral and expanding up to $\mathcal{O}(\epsilon^0)$,

$$\begin{aligned}\mathcal{S}_{c\rho_\alpha}^{\text{opp}[i]}(\rho_\alpha^c) &= C_i \left\{ \frac{1}{4\epsilon^2} A \left(\frac{\mu^2}{(Q\rho_\alpha^c)^2} \frac{4\alpha}{(1+\alpha)^2} \right)^{2\epsilon} F_0 - \left(\frac{\alpha_s}{2\pi} \right)^2 \frac{1}{4\epsilon} \left(\frac{\mu^2}{(Q\rho_\alpha^c)^2} \frac{4\alpha}{(1+\alpha)^2} \right)^{2\epsilon} \int_0^\infty \frac{dr}{r} F_1(r) \right. \\ &\quad \left. + \frac{1}{2} \left(\frac{\alpha_s}{2\pi} \right)^2 \theta(\rho_\alpha^c) \int_0^{1/\alpha} \frac{dr}{r} \ln(r\alpha) F_1(r) + \frac{1}{2} \left(\frac{\alpha_s}{2\pi} \right)^2 \theta(\rho_\alpha^c) \int_0^\alpha \frac{dr}{r} \ln(r/\alpha) F_1(r) \right\}.\end{aligned}\quad (4.19)$$

From this result we find the non-global structure in the last two terms is equivalent to the corresponding non-global structure in the double cumulant, Eq. (4.10), with the replacement $\ell_1^c/\ell_2^c \rightarrow \alpha$.

We can go through the same procedure for asymmetric thrust, whose cumulant is

$$\mathcal{S}_{c\tau_\alpha}^{\text{opp}}(\tau_\alpha^c) = \int_0^{\tau_\alpha^c} d\tau_\alpha \int d\ell_1 d\ell_2 \delta\left(\tau_\alpha - \frac{2}{1+\alpha} \frac{\alpha\ell_1 + \ell_2}{Q}\right) S^{\text{opp}}(\ell_1, \ell_2, \mu). \quad (4.20)$$

In terms of integrals over s and r ,

$$\mathcal{S}_{c\tau_\alpha}^{\text{opp}}(\tau_\alpha^c) = \int_0^\infty \frac{dr}{2r} \int_0^{s^c} ds S^{\text{opp}}(\ell_1, \ell_2, \mu), \quad (4.21)$$

where

$$s^c = \frac{(Q\tau_\alpha^c)^2(1+\alpha)^2}{4\alpha(\alpha r + 1/(\alpha r) + 2)}. \quad (4.22)$$

Evaluating the s integral and expanding to finite terms,

$$\begin{aligned} \mathcal{S}_{c\tau_\alpha}^{\text{opp}[i]}(\tau_\alpha^c) = C_i \left\{ -\frac{1}{4\epsilon} \frac{\Gamma(-2\epsilon)^2}{\Gamma(-4\epsilon)} A \left(\frac{\mu^2}{(Q\tau_\alpha^c)^2} \frac{4\alpha}{(1+\alpha)^2} \right)^{2\epsilon} F_0 \right. \\ \left. - \frac{1}{4\epsilon} \left(\frac{\alpha_s}{2\pi} \right)^2 \left(\frac{\mu^2}{(Q\tau_\alpha^c)^2} \frac{4\alpha}{(1+\alpha)^2} \right)^{2\epsilon} \int_0^\infty \frac{dr}{r} F_1(r) \right. \\ \left. - \frac{1}{2} \left(\frac{\alpha_s}{2\pi} \right)^2 \theta(\tau_\alpha^c) \int_0^\infty \frac{dr}{r} \ln \left(\alpha r + \frac{1}{\alpha r} + 2 \right) F_1(r) \right\}. \quad (4.23) \end{aligned}$$

Although the non-global structure in this result is less obvious, we know from the position space result that the non-global structure in α for τ_α is functionally equivalent to the non-global structure in $t_2(x_1/x_2)$, the position space form of the non-global terms in the soft function.

To conclude, we have shown that the non-global structure in the hemisphere soft function in position space and momentum space are reproduced by the asymmetric thrust and asymmetric heavy jet mass observables respectively.

4.3 Heavy Jet Mass and Thrust

For heavy jet mass ρ_H and thrust $T = 1 - \tau$ we will compute the difference of the cumulants of the non-global terms at $\mathcal{O}(\alpha_s^2)$. This corresponds to the projection of $t_2(x_1, x_2)$ in position space, Eq. (2.13). From Eqs. (4.14) and (4.16) with $\alpha = 1$ this simply gives constant terms in the cumulants, which are $\delta(\rho_H)$ and $\delta(\tau)$ terms in the corresponding distributions. Since we will take the difference of heavy jet mass and thrust we only need opposite hemisphere terms. We examine the projections in both momentum space and position space. The results are the same, providing an internal consistency check on our position and momentum space results, and more importantly the analytic results for the projection match the numerical extraction of these constants from EVENT2, which were discussed in Sec. 2.3. We call Σ_H the heavy jet mass cumulant and Σ_τ the thrust cumulant, and add a superscript NG to refer to keeping only the terms in the cumulants induced by the non-global structure at $\mathcal{O}(\alpha_s^2)$.

4.3.1 Projection From Position Space

Taking the $\alpha = 1$ result for the asymmetric heavy jet mass projection from Eq. (4.16) to find the projection for the non-global terms,

$$\Sigma_H^{\text{NG}}(\rho) = \frac{\alpha_s^2}{8\pi^2} \theta(\rho) \int_0^\pi \frac{d\theta}{\pi} t_2(e^{i\theta}) = \frac{\alpha_s^2}{8\pi^2} \theta(\rho) \left[C_F C_A s_{2\rho}^{[C_F C_A]} + C_F T_R n_f s_{2\rho}^{[n_f]} \right], \quad (4.24)$$

where we used $t_2(e^{i\theta}) = t_2(e^{-i\theta})$. Similarly, we can take the $\alpha = 1$ result for the asymmetric thrust projection from Eq. (4.14):

$$\Sigma_\tau^{\text{NG}}(\tau) = \frac{\alpha_s^2}{8\pi^2} \theta(\tau) t_2(1) = \frac{\alpha_s^2}{8\pi^2} \theta(\tau) \left[C_F C_A s_2^{[C_F C_A]} + C_F T_R n_f s_2^{[n_f]} \right]. \quad (4.25)$$

Therefore the difference in cumulants is

$$\begin{aligned}\Sigma_H^{\text{NG}}(\rho) - \Sigma_\tau^{\text{NG}}(\rho) &= \frac{\alpha_s^2}{8\pi^2} \theta(\rho) \int_0^\pi \frac{d\theta}{\pi} \left(t_2(e^{i\theta}) - t_2(1) \right) \\ &= \frac{\alpha_s^2}{8\pi^2} \theta(\rho) \left[C_F C_A (s_{2\rho} - s_2)^{[C_F C_A]} + C_F T_R n_f (s_{2\rho} - s_2)^{[n_f]} \right],\end{aligned}\tag{4.26}$$

which provides an alternate derivation of Eq. (2.22). We will use the momentum space projection to determine the analytic value for the difference in cumulants, as the integrals are more straightforward.

4.3.2 Projection from Momentum Space

In momentum space, we can take the $\alpha = 1$ results for asymmetric heavy jet mass and asymmetric thrust, given in Eqs. (4.19) and (4.23) respectively. When we take the difference of the bare results, all of the ϵ and μ dependence cancels, as these terms are equal in the two distributions. What remains are the finite terms that are the difference in constants for the two distributions:

$$\begin{aligned}\Sigma_H^{\text{NG}}(\rho) - \Sigma_\tau^{\text{NG}}(\rho) &= \left(\frac{\alpha_s}{2\pi} \right)^2 \theta(\rho) C_i \left(\frac{\pi^2}{6} F_0 + 2 \int_0^1 \frac{dr}{r} \ln(1+r) F_1(r) \right) \\ &= \frac{\alpha_s^2}{8\pi^2} \theta(\rho) \left[C_F C_A (s_{2\rho} - s_2)^{[C_F C_A]} + C_F T_R n_f (s_{2\rho} - s_2)^{[n_f]} \right],\end{aligned}\tag{4.27}$$

where the $s_{2\rho}^{[a]}$ and $s_2^{[a]}$ constants are defined in Eqs. (2.17) and (2.20). Note that $-\frac{1}{2}F_0$ gives the coefficient of the non-global double log term in the hemisphere soft function. Using the results in Appendix B we find

$$\begin{aligned}\Sigma_H(\rho) - \Sigma_\tau(\rho) &= \frac{\alpha_s^2}{8\pi^2} \theta(\rho) \left[C_F T_R n_f \left(4\zeta_3 - \frac{4}{3} \right) + C_F C_A \left(\frac{2}{3} + \frac{19\pi^4}{45} + \frac{2\pi^2}{3} \ln^2 2 \right. \right. \\ &\quad \left. \left. - \frac{2}{3} \ln^4 2 - 16 \text{Li}_4 \left(\frac{1}{2} \right) - 11\zeta_3 - 14\zeta_3 \ln 2 \right) \right].\end{aligned}\tag{4.28}$$

This yields the analytic result quoted above in Eq. (3.40), and agrees with a numerical evaluation of the projection in Eq. (4.26) using our analytic position space result. Numerically Eq. (4.28) gives

$$(s_{2\rho} - s_2)^{[C_F C_A]} = 11.6352, \quad (s_{2\rho} - s_2)^{[n_f]} = 3.4749\tag{4.29}$$

which can be compared to the EVENT2 extractions in Eq. (2.23). There is excellent agreement between our analytic results and the EVENT2 extractions, providing a strong consistency check on our calculation.

The constant $s_{2\rho} - s_2$ has contributions from both the non-global logarithms and the remaining non-global terms. For each color structure, the contributions from each set of terms is

| | $C_F C_A$ | $C_F T_R n_f$ | |
|-------------|-----------|---------------|--------|
| double log: | 43.293 | — | (4.30) |
| single log: | 39.586 | −15.791 | |
| non-log: | −59.609 | 22.741 . | |

We see that the non-global logs do not dominate the contribution, and the full set of non-global terms is needed to accurately determine the constant.

5. Two Dimensional Comparison with EVENT2

The Monte Carlo EVENT2 [23, 24] allows us to study the structure of the hemisphere jet mass distribution. EVENT2 contains the matrix elements necessary to compute dijet event shapes at $\mathcal{O}(\alpha_s^2)$, and it allows us to numerically compute the non-global contributions in the hemisphere mass distribution. We use the program to numerically compute the distribution of m_2^2 making the cut $m_1^2 < m_1^{c2}$:

$$\frac{d\sigma}{dm_2^2}(m_1^{c2}) = \int_0^{m_1^{c2}} dm_1^2 \frac{d^2\sigma}{dm_1^2 dm_2^2}. \quad (5.1)$$

In the region $m_2^2 \ll m_1^{c2} \ll Q^2$, the dijet factorization theorem we use here applies, and we can compare the results of EVENT2 in this regime to our calculation. In Sec. 5.1 we compare the soft non-global logarithms from EVENT2 with our calculation and show there is excellent agreement.

When $m_2^2 \ll m_1^{c2} \sim Q^2$, our factorization theorem does not apply and a new source of non-global logarithms, hard non-global logarithms, arises. In Sec. 5.2 we use EVENT2 to show that these hard non-global logs exist. These new hard non-global logs would require a new set of analytic calculations to understand.

5.1 Soft Non-Global Logarithms

In this section we perform a direct comparison of our hemisphere soft function with the Monte Carlo program EVENT2. The distribution in Eq. (5.1) is related to the double cumulant in m_1^2 and m_2^2 , $\Sigma(m_1^{c2}, m_2^2)$. For a bin in m_2^2 between $m_{2,\min}^2$ and $m_{2,\max}^2$, the value of the distribution in the bin will be

$$\begin{aligned} & \Sigma(m_1^{c2}, m_{2,\max}^2) - \Sigma(m_1^{c2}, m_{2,\min}^2) \\ &= \int_0^{m_1^{c2}} dm_1^2 \int_0^{m_{2,\max}^2} dm_2^2 \frac{d^2\sigma}{dm_1^2 dm_2^2} - \int_0^{m_1^{c2}} dm_1^2 \int_0^{m_{2,\min}^2} dm_2^2 \frac{d^2\sigma}{dm_1^2 dm_2^2}. \end{aligned} \quad (5.2)$$

This double cumulant is for the full distribution, meaning it is a sum of the global terms in the distribution, the non-global terms that we have determined, and terms that are power suppressed by $m_i^2/Q^2 \ll 1$. To test our analytic results we will make use of the double cumulant for the non-global terms given in Eq. (3.35). The region we are interested in to avoid power corrections and obtain sensitivity to non-global logs is

$$m_2^2 \ll m_1^{c2} \ll Q. \quad (5.3)$$

As $m_1^c \rightarrow Q$, we are inclusive over a region of phase space where a hard non-global logarithm can contribute, i.e. $m_2^2 \ll m_1^{c2} \sim Q$. These hard non-global logs are non-singular in m_1 , e.g., $m_1 \ln(m_2/Q)$. As we vary m_1^{c2} in the program, we observe the effects of such terms, and we can turn them off by choosing $m_1^{c2} \ll Q^2$.

In our comparison to EVENT2 we focus on the $C_F C_A$ and $C_F T_R n_f$ color structures, as the form of the C_F^2 color structure is constrained by exponentiation. To compare our calculation with the soft non-global logarithms in the double hemisphere mass distribution,

we subtract the full dependence in these color structures for the double hemisphere mass distribution from EVENT2.

The level of numeric accuracy in the doubly differential distribution required to resolve the contribution of the non-global terms is significant. To achieve this accuracy for the $C_F C_A$ terms we ran EVENT2 with 1.82×10^{12} events. Additionally for the $C_F C_A$ color structure, we chose the parameters $\text{CUTOFF} = 10^{-15}$ and $\text{NPOW1} = \text{NPOW2} = 3$. The choice of CUTOFF allows us to reliably sample m_2^2 down to $\log_{10} m_2^2/Q^2 = 10^{-7}$ and the choices of NPOW1 and NPOW2 significantly reduce the statistical uncertainties compared to the default choices $\text{NPOW1} = \text{NPOW2} = 2$. For the $C_F T_R n_f$ color structure, we found that taking $\text{NPOW1} = \text{NPOW2} = 4$ was necessary to obtain reliable results, and with this parameter choice we ran 0.253×10^{12} events. This choice of parameters, though, introduces large systematic and statistical errors into the large m_2^2 region of the distribution. It appears to be more delicate to compare the results of EVENT2 for this color structure with our calculation.

The full set of terms contributing to the distribution can be divided up into groups. In the limit we are working, the cumulant terms can be divided up as

$$\Sigma = \Sigma^{\text{global}} + \Sigma^{\ln^2} + \Sigma^{\ln} + \Sigma^{\text{NG}} + \Sigma^{\text{p.c.}}. \quad (5.4)$$

The global singular terms determined by RG evolution in the dijet hemisphere factorization theorem, are in Σ^{global} . The non-global double and single log terms are in Σ^{\ln^2} and Σ^{\ln} , and the remaining non-global non-log terms are contained in Σ^{NG} . Here Σ^{\ln} and Σ^{NG} are determined by our calculation. Additionally, there are power corrections to the dijet limit that sit in $\Sigma^{\text{p.c.}}$ and contribute in EVENT2, but which are not known analytically.

For both of the color structures $C_F C_A$ and $C_F T_R n_f$ we will show the distribution in m_2^2 from EVENT2 with a cut on m_1^2 , $d\sigma_{\text{EV2}}/dm_2^2(m_1^{c2})$, with various terms subtracted. We choose the cut in m_1 to be

$$m_1^{c2}/Q^2 = 9.2 \times 10^{-4}, \quad \log_{10}(m_1^{c2}/Q^2) = -3.0. \quad (5.5)$$

Specifically, in Figs. 5 and 6 we plot the distributions

$$\begin{aligned} \text{(top-left)} \quad & \frac{d\sigma_{\text{EV2}}}{dm_2^2}(m_1^{c2}), \\ \text{(top-right)} \quad & \frac{d\sigma_{\text{EV2}}}{dm_2^2}(m_1^{c2}) - \frac{d\sigma_{\text{global}}}{dm_2^2}(m_1^{c2}), \\ \text{(bottom-left)} \quad & \frac{d\sigma_{\text{EV2}}}{dm_2^2}(m_1^{c2}) - \frac{d\sigma_{\text{global}}}{dm_2^2}(m_1^{c2}) - \frac{d\sigma_{\ln^2}}{dm_2^2}(m_1^{c2}) \quad \text{for } C_F C_A, \\ & \frac{d\sigma_{\text{EV2}}}{dm_2^2}(m_1^{c2}) - \frac{d\sigma_{\text{global}}}{dm_2^2}(m_1^{c2}) - \frac{d\sigma_{\ln}}{dm_2^2}(m_1^{c2}) \quad \text{for } C_F T_R n_f, \\ \text{(bottom-right)} \quad & \frac{d\sigma_{\text{EV2}}}{dm_2^2}(m_1^{c2}) - \frac{d\sigma_{\text{global}}}{dm_2^2}(m_1^{c2}) - \frac{d\sigma_{\ln^2}}{dm_2^2}(m_1^{c2}) - \frac{d\sigma_{\text{NG}}}{dm_2^2}(m_1^{c2}). \end{aligned} \quad (5.6)$$

In Fig. 5 we show the distributions in Eq. (5.6) for the $C_F C_A$ color structure. Note that a non-zero flat region in the distribution indicates the presence of a single log of m_2^2 , while

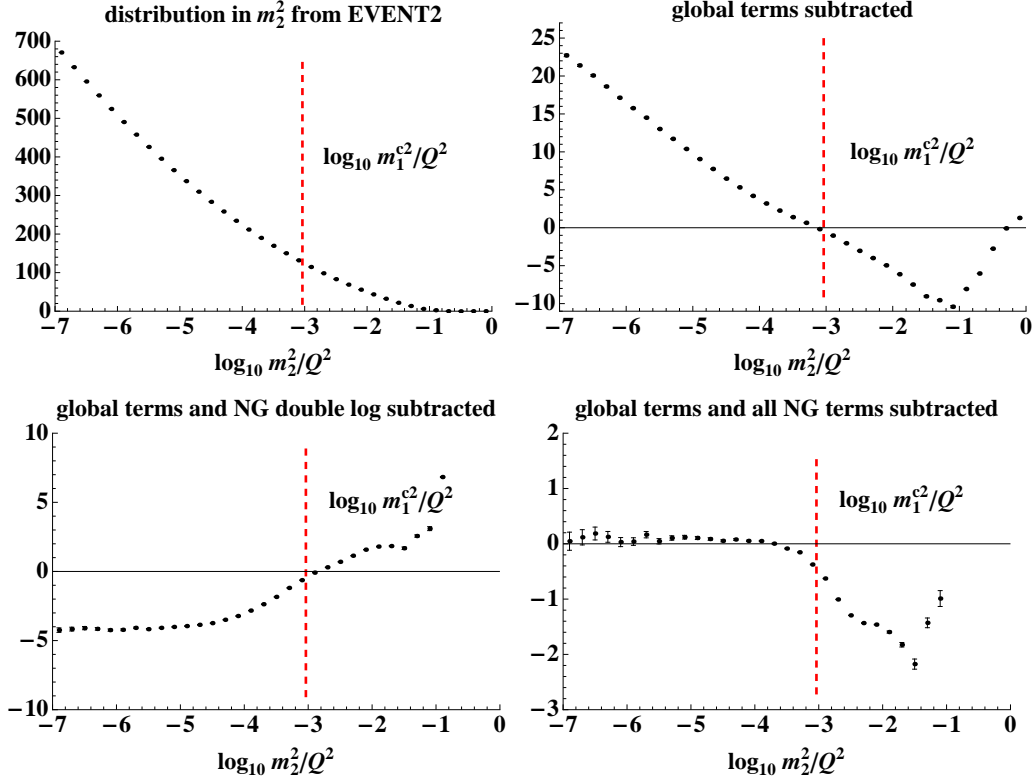


Figure 5: The $\mathcal{O}(\alpha_s^2)$, $C_F C_A$ distribution from EVENT2 with various sets of terms removed. The upper left plot shows the distribution directly from EVENT2. The upper right plot has the known global terms subtracted, and the lower left plot has both the global terms and the known non-global double log subtracted. The lower right plot has the global terms and the non-global terms from our calculation subtracted. The red line marks the value of m_1^c used. Note the changing vertical scale between the plots.

a line with non-zero slope indicates the presence of a double log of m_2^2 . We can clearly see that after we subtract the global terms a double log remains. Once we subtract this double log coming from Σ^{\ln^2} , the remaining distribution still has a single log of m_2^2 . This single log is in Σ^{NG} , and once we remove these terms the residual distribution for $m_2^2 \ll m_1^c$ for the $C_F C_A$ terms is very small compared to the size of the non-global terms. We expect that power corrections in m_1^c/Q^2 account for the remaining tiny discrepancy from zero.

The nice agreement with EVENT2 for the $C_F C_A$ color structure is a very strong check on our calculation. The m_2^2 dependence of the $C_F C_A$ distribution has been fully accounted for by our calculation of the non-global terms, up to a very small correction likely arising from power corrections in m_1^c/Q^2 .

In Fig. 6 we show the distributions in Eq. (5.6) for the $C_F T_{Rn_f}$ color structure. Note that there is no double log term to subtract for this color structure, so the lower left plot subtracts the single log. Recall that the parameter choice $\text{NPOW1} = \text{NPOW2} = 4$, needed

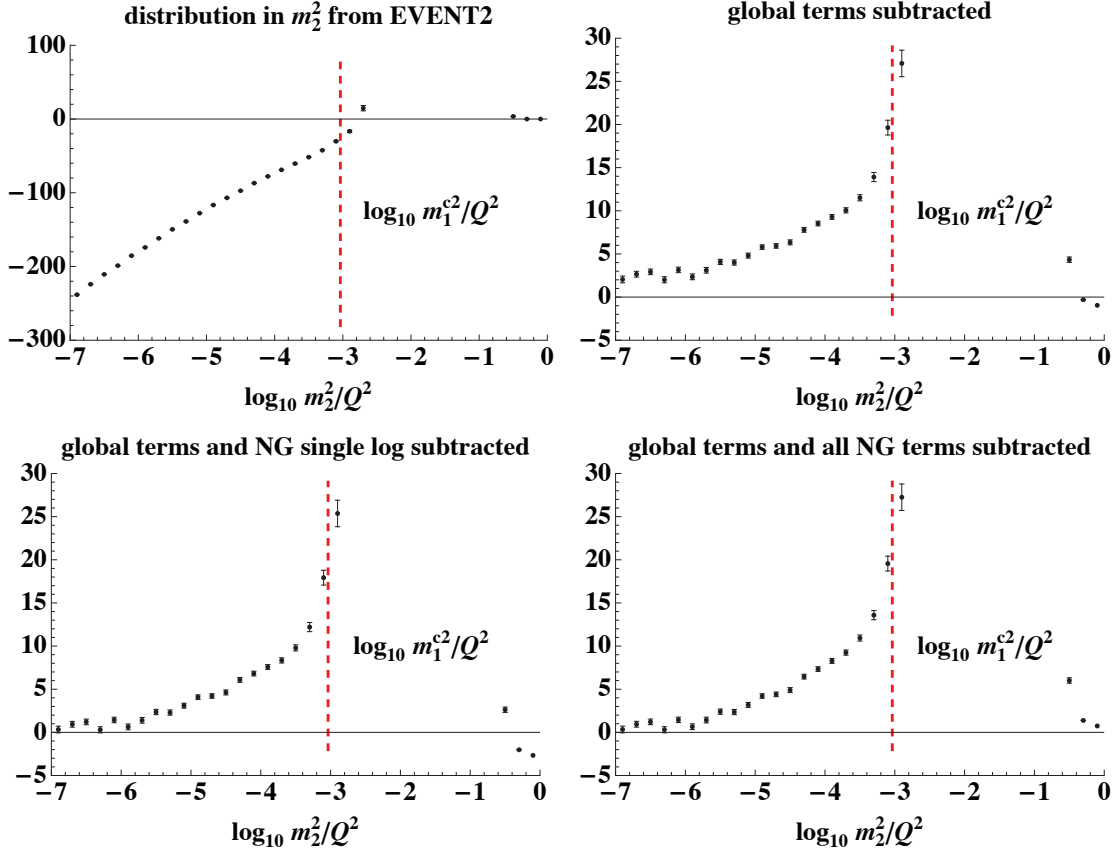


Figure 6: The $\mathcal{O}(\alpha_s^2)$, C_{FTRNf} distribution from EVENT2 with various sets of terms removed, as in Fig. 5. The upper left plot shows the distribution directly from EVENT2. The upper right plot has the known global terms subtracted. The lower left plot is the same as the upper right, since there is no non-global double log to subtract. The lower right plot has the global terms and the non-global terms from our calculation subtracted. The red line marks the value of m_1^c used. Note the changing vertical scale between the plots. The high region of the distribution has large numerical errors; see the discussion in the text for more details.

for reliability in the small m_2^2 region, has introduced large statistical and systematic errors in the large m_2^2 region, to the point that there is a clear deviation of the EVENT2 results away from the true distribution for $m_2^2/Q^2 > 10^{-3}$. However, we still see consistency between our calculation and the EVENT2 results in the small m_2^2 region. These uncertainties at large m_2^2 make the result less definitive as the C_{FC_A} color structure, but it nonetheless gives us confidence in our results.

5.2 Hard Non-Global Logarithms

We have seen that our calculation of the soft non-global logarithms from our calculation match well to the results of EVENT2. These soft non-global logs appear in the region of phase space where

$$m_2^2 \ll m_1^{c2} \ll Q^2. \quad (5.7)$$

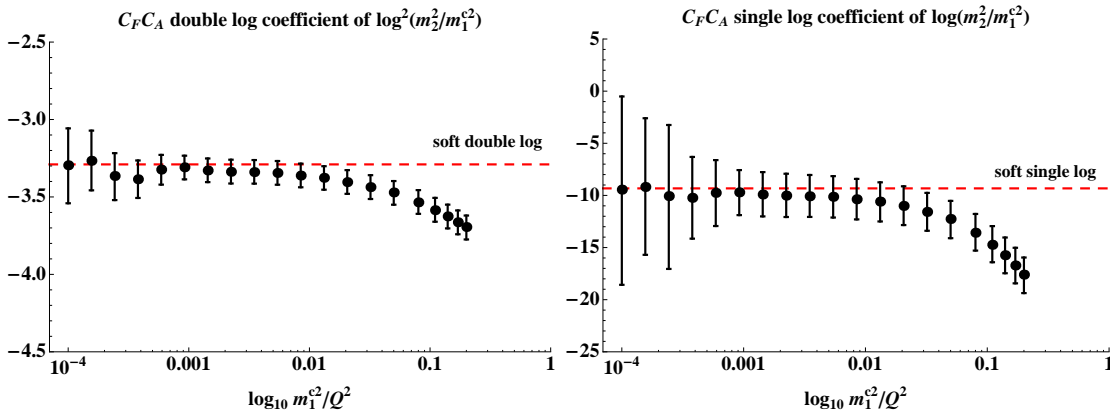


Figure 7: The coefficient of the double and single logarithms of m_2^2/m_1^{c2} extracted from EVENT2. We have taken the distribution in Eq. (5.1) and subtracted the non-global non-logarithmic structure from our calculation and fit to the coefficient of the double and single logarithms of m_2^2/m_1^{c2} . For $m_1^{c2} \ll Q^2$, the coefficients of these logarithms agree with the soft non-global logarithms in our calculation. However, as m_1^{c2} increases, we see the coefficients of these logarithms change away from the soft limit, demonstrating the presence of hard non-global logarithms.

Non-global logs can arise in other regions of phase space, and the non-global structure in these regions can be different. Hard non-global logs arise from a region of phase space where one jet mass is large,

$$m_2^2 \ll m_1^{c2} \sim Q^2. \quad (5.8)$$

In this regime there are two types of large logarithms:

$$\ln\left(\frac{m_2^2}{m_1^{c2}}\right), \quad \ln\left(\frac{m_2^2}{Q^2}\right). \quad (5.9)$$

We fit to the form of the first type of logarithm, $\ln(m_2^2/m_1^{c2})$, while varying the upper limit on m_1^{c2} on the mass of the heavier jet. If there were no new sources of non-global logarithms, then we would find that the coefficients of the double and single logarithms were the same as the soft non-global logarithms from our calculation. Any new hard non-global logs require a new set of calculations to understand, as the factorization theorem we use to investigate soft non-global logs only applies in the limit $m_1^{c2}, m_2^2 \ll Q^2$.

We can use EVENT2 to investigate the appearance of hard non-global logarithms, and in Fig. 7 we use EVENT2 to show their existence for the first time. We study only the $C_F C_A$ color structure, as this distribution was more straightforward to compare for the soft non-global logarithms. To study hard non-global logs in EVENT2, we calculate the distribution in m_2^2 with a cut $m_1^2 < m_1^{c2}$, as in Eq. (5.1). We take a broad set of m_1^{c2} values, ranging from $m_1^{c2} = 1 \times 10^{-4}$ to 0.2 ⁴. For each value of m_1^{c2} we fit to determine the coefficients of the double and single logarithms of m_2^2/m_1^{c2} . This fit amounts to determining the slope and intercept of the distributions like those plotted in Figs. 5 and 6 (which for brevity we do not show here).

⁴The data set that we have used for this study as 0.360×10^{12} events with $CUTOFF = 10^{-15}$ and $NPOW1 = NPOW2 = 2$.

The results in Fig. 7 clearly show that the coefficient of $\ln^2(m_2^2/m_1^2)$ and of $\ln(m_2^2/m_1^2)$ both change as a function of m_1^2/Q^2 . The deviation of these coefficients from the dashed lines in the figure implies the existence of hard non-global logarithms. The structure of these hard non-global logs warrants further study.

6. Conclusions, Simple Generalizations, and Outlook

We have calculated the dijet hemisphere soft function to order α_s^2 in both position and cumulant momentum space, $\tilde{S}(x_1, x_2, \mu)$ and $\mathcal{S}_c(\ell_1^c, \ell_2^c, \mu)$. In doing so, we uncovered the full non-global structure of these functions, that is, the dependence on the ratios x_1/x_2 or ℓ_1^c/ℓ_2^c which is not fixed by renormalization group invariance of the factorized dijet cross section Eq. (1.4). We re-derived the non-global double logarithm whose presence in related observables was pointed out by [20], obtained new results for the single logarithmic terms, as well as determining the full non-logarithmic non-global structure in the dijet soft function and related observables. Eqs. (3.30) and (3.35) are the main results of this paper. These results go significantly beyond previous discussion of non-global structures in jet cross sections at $\mathcal{O}(\alpha_s^2)$. We also demonstrated numerically the existence of hard non-global double and single logs in double hemisphere mass distributions when $m_2^2 \ll m_1^2 \sim Q^2$.

The discovery of these non-global structures resolves the question of the structure of the dijet soft function. The ansatz of Ref. [39] that only double logarithms of x_1/x_2 and a constant could exist in $\tilde{S}(x_1, x_2, \mu)$ due in part to $x_1 \leftrightarrow x_2$ symmetry, is incomplete. Many other functions of x_1/x_2 appear, including a single logarithm $\ln(x_1/x_2 + x_2/x_1)$ that is symmetric under $x_1 \leftrightarrow x_2$.

A key piece of our strategy to simplify calculation of the dijet soft function was to take advantage of renormalization group properties and infrared finiteness of the full soft function $\tilde{S}(x_1, x_2, \mu)$ or $S(\ell_1, \ell_2, \mu)$ so that all the non-global dependence at $\mathcal{O}(\alpha_s^2)$ could be extracted only from those diagrams in which two particles in the final state enter opposite hemispheres of the dijet event. This procedure determines all the terms in the soft function except for the constant term, which we take from a recent calculation of this constant in the $\mathcal{O}(\alpha_s^2)$ thrust distribution by [37]. Cancellation of IR divergences between same and opposite hemisphere final state configurations leaves over logs of x_1/x_2 or ℓ_1/ℓ_2 , illuminating how NGLs find their origin in the structure of a soft function [45].

We performed several cross-checks of our result, by considering general covariant gauge, by projecting the dijet soft function onto various observables and comparing to EVENT2 predictions for those observables. These comparisons revealed existing EVENT2 extractions for the difference between heavy jet mass and thrust soft function constants to be in excellent agreement with our analytic result. We also compared our prediction for the double hemisphere mass distribution to our own EVENT2 runs, and again found good agreement.

State of the art fits for α_s from $e^+e^- \rightarrow$ jet data currently rely on N³LL resummations of event shape distributions [16, 22, 18] and thus on the fixed-order $\mathcal{O}(\alpha_s^2)$ dijet soft function. Our new results make possible improved extractions of the strong coupling by removing a source of uncertainty in the perturbative calculation.

The $\mathcal{O}(\alpha_s^2)$ soft function in position space, in particular, makes possible a fully analytic N³LL resummation of the doubly differential cross section Eq. (1.10) in position space when $x_1/x_2 \sim 1$, and is also a crucial ingredient in the N³LL resummation of the doubly differential momentum space distribution Eq. (1.4) or cumulant Eq. (1.5).

One simple generalization of our results is to the case of hadron colliders. For pp and $p\bar{p}$ collisions an incoming dijet hemisphere soft function appears for the event shape called beam thrust τ_B (or 0-jettiness), which in the dijet limit $\tau_B \ll 1$ provides a veto on central jets. This only difference between our soft function in Eq. (2.4) and the incoming one are that the Wilson lines are incoming from $-\infty$ rather than outgoing to $+\infty$. This reflects itself in the signs of $i0^+$ factors in the eikonal denominators in the momentum space amplitudes. Since for our opposite hemisphere calculation the signs of those $i0^+$ factors drops out, our analytic results for the x_1/x_2 and ℓ_1^c/ℓ_2^c dependence immediately carries over to the incoming case. In Ref. [47] it was proven that the μ dependent logarithms are also the same for the outgoing and incoming dijet hemisphere soft functions. Hence at $\mathcal{O}(\alpha_s^2)$ the only thing that can differ between the two cases is the thrust constant $s_2^{[C_F C_A, n_f]}$. (It would be interesting to compute these constants directly for the incoming case.) Thus our results already make possible an improvement of predictions for jet observables in hadron collisions.

Another simple generalization of our results are to Wilson lines in different color representations, such as octets for incoming or outgoing gluon dijets. It is straightforward to see that our computations obey Casimir scaling, so we can simply modify the C_F 's to get results for other representations. For the \mathcal{G} , \mathcal{H} , and \mathcal{Q} graphs only traces that obey Casimir scaling appear. For the \mathcal{I} and \mathcal{T} graphs non-abelian exponentiation and the generator commutation relations guarantee that Casimir scaling also applies.

Looking ahead, relating non-global logarithms to the soft function in a factorization theorem in the context of effective field theory as we have done also opens the door to the development of renormalization group techniques to resum non-global logarithms. This would make it possible to go beyond the resummation of NGLs in the conjectured form given in [20] which is parameterized in terms of coefficients determined numerically in the large- N_C limit. It is important to keep in mind that such NGLs (and other non-global structures as we found here) will appear not only in the single or double-hemisphere mass distributions, but also in most jet cross sections in which jets are defined with one of the well known jet algorithms, which leave the regions inside and outside these jets sensitive to different soft scales [29, 45].

Note added: While this paper was being finalized, Ref. [48] appeared calculating the dijet hemisphere soft function in momentum space, $\mathcal{S}_c(\ell_1^c, \ell_2^c, \mu)$. Although the result for $\mathcal{S}_c(\ell_1^c, \ell_2^c, \mu)$ has a different form than our result in Eq. (3.35) the two exactly agree numerically. In our result the logarithmic singularities are separated out explicitly and the remaining polylog dependent contributions [our $f(\ell_1^c/\ell_2^c) + f(\ell_2^c/\ell_1^c)$ given by Eq. (3.36)] are bounded, unlike the result in Ref. [48]. Ref. [48] does in addition compute analytically the thrust constants, unlike our paper, finding $s_2^{[C_F C_A]} = -\frac{1070}{81} - \frac{871}{108}\pi^2 + \frac{7}{15}\pi^4 + \frac{143}{9}\zeta_3$ and $s_2^{[n_f]} = \frac{40}{81} + \frac{77}{27}\pi^2 - \frac{52}{9}\zeta_3$, which agree numerically with the first four digits of the result

from Ref. [37] quoted in Eq. (2.19). An analog of our two dimensional position space result $S(x_1, x_2, \mu)$ in Eq. (3.30) was not obtained in Ref. [48].

Acknowledgments

The authors would like to thank the University of California at Berkeley, Lawrence Berkeley National Laboratory, Massachusetts Institute of Technology, University of Washington and Harvard University for hospitality during portions of this work, and CL would like to thank the Aspen Center for Physics for the same. IS thanks M. Schwartz for useful discussion. This work is supported in part by the Offices of Nuclear and High Energy Physics of the U.S. Department of Energy under Contracts DE-FG02-94ER40818, DE-FGO3-96-ER40956, DE-SC003916, and DE-FGO3-96-ER40956. The work of JW was supported in part by a LHC Theory Initiative Postdoctoral Fellowship, under the National Science Foundation grant PHY-0705682, and that of IS by the Alexander von Humboldt foundation.

A. Anomalous Dimensions

In Sec. 2.2 we reviewed how the μ -dependent terms in the soft function can be constrained using renormalization group invariance of the cross section Eq. (1.4). Here we record the soft anomalous dimensions that are needed to carry this out explicitly to $\mathcal{O}(\alpha_s^2)$.

The exponents K, ω appearing in the evolution factors $U_S(x, \mu, \mu_0)$ in Eq. (2.10) are defined by

$$K(\Gamma_{\text{cusp}}, \gamma_S, \mu, \mu_0) = \int_{\mu_0}^{\mu} \frac{d\mu'}{\mu'} \left(-2\Gamma_{\text{cusp}}[\alpha_s(\mu')] \ln \frac{\mu'}{\mu_0} + \gamma_S[\alpha_s(\mu')] \right), \quad (\text{A.1a})$$

$$\omega(\Gamma_{\text{cusp}}, \mu, \mu_0) = -2 \int_{\mu_0}^{\mu} \frac{d\mu'}{\mu'} \Gamma_{\text{cusp}}[\alpha_s(\mu')], \quad (\text{A.1b})$$

where the cusp and non-cusp parts of the anomalous dimension Γ_{cusp} and γ_S are defined by Eq. (2.8). We define the expansions of the anomalous dimensions in α_s as

$$\Gamma_{\text{cusp}}[\alpha_s] = \sum_{k=0}^{\infty} \left(\frac{\alpha_s}{4\pi} \right)^{k+1} \Gamma_{\text{cusp}}^k, \quad \gamma_S[\alpha_s] = \sum_{k=0}^{\infty} \left(\frac{\alpha_s}{4\pi} \right)^{k+1} \gamma_S^k. \quad (\text{A.2})$$

At $\mathcal{O}(\alpha_s)$ and $\mathcal{O}(\alpha_s^2)$ [49, 50], the cusp anomalous dimension is given by

$$\Gamma_{\text{cusp}}^0 = 4C_F \quad (\text{A.3a})$$

$$\Gamma_{\text{cusp}}^1 = 4C_F C_A \left(\frac{67}{9} - \frac{\pi^2}{3} \right) - C_F T_R n_f \frac{80}{9}, \quad (\text{A.3b})$$

and the non-cusp anomalous dimension is given by

$$\gamma_S^0 = 0 \quad (\text{A.4a})$$

$$\gamma_S^1 = C_F C_A \left(-\frac{808}{27} + \frac{11\pi^2}{9} + 28\zeta_3 \right) + C_F T_R n_f \left(\frac{224}{27} - \frac{4}{9}\pi^2 \right). \quad (\text{A.4b})$$

We also need the coefficients of the beta function,

$$\beta[\alpha_s] = \sum_{k=0}^{\infty} \left(\frac{\alpha_s}{4\pi} \right)^{k+1} \beta_k, \quad (\text{A.5})$$

where

$$\beta_0 = \frac{11}{3}C_A - \frac{4}{3}T_R n_f, \quad (\text{A.6a})$$

$$\beta_1 = \frac{34}{3}C_A^2 - \frac{20}{3}C_A T_R n_f - 4C_F T_R n_F. \quad (\text{A.6b})$$

In terms of these beta function coefficients, the two-loop running coupling is given by

$$\frac{1}{\alpha_s(\mu')} = \frac{1}{\alpha_s(\mu)} + \frac{\beta_0}{2\pi} \ln \frac{\mu'}{\mu} + \frac{\beta_1}{4\pi\beta_0} \ln \left[1 + \frac{\beta_0}{2\pi} \alpha_s(\mu) \ln \frac{\mu'}{\mu} \right] \quad (\text{A.7})$$

These are all the quantities needed to determine the μ -dependent pieces of the soft function to $\mathcal{O}(\alpha_s^2)$.⁵

The quantities K, ω to $\mathcal{O}(\alpha_s^2)$ written out explicitly are

$$K(\Gamma_{\text{cusp}}, \gamma_S, \mu, \mu_0) = \frac{\alpha_s(\mu)}{4\pi} \left(-\Gamma_{\text{cusp}}^0 \ln^2 \frac{\mu}{\mu_0} + \gamma_S^0 \ln \frac{\mu}{\mu_0} \right) \quad (\text{A.8a})$$

$$+ \left(\frac{\alpha_s(\mu)}{4\pi} \right)^2 \left[-\frac{2}{3} \Gamma_{\text{cusp}}^0 \beta_0 \ln^3 \frac{\mu}{\mu_0} + (\gamma_S^0 \beta_0 - \Gamma_{\text{cusp}}^1) \ln^2 \frac{\mu}{\mu_0} + \gamma_S^1 \ln \frac{\mu}{\mu_0} \right]$$

$$\omega(\Gamma_{\text{cusp}}, \mu, \mu_0) = \left(\frac{\alpha_s(\mu)}{4\pi} \right) \left(-2\Gamma_{\text{cusp}}^0 \ln \frac{\mu}{\mu_0} \right) \quad (\text{A.8b})$$

$$- \left(\frac{\alpha_s(\mu)}{4\pi} \right)^2 \left(\frac{\Gamma_{\text{cusp}}^0 \beta_0}{2} \ln^2 \frac{\mu}{\mu_0} + \frac{\Gamma_{\text{cusp}}^1}{2} \ln \frac{\mu}{\mu_0} \right).$$

These expressions can be used to determine the parts of the soft function dependent on logs of μ , Eq. (3.34) in position space and Eq. (3.41) for the double cumulant in momentum space.

B. $\mathcal{O}(\alpha_s^2)$ Diagram Results for the Opposite Hemisphere Soft Function

Here we present the details of our calculation of the $\mathcal{O}(\alpha_s^2)$ opposite hemisphere soft function, in both position and momentum space. The opposite hemisphere soft function in momentum space is given by

$$S^{\text{OPP}}(\ell_1, \ell_2) = \sum_j \int \frac{d^d k_1}{(2\pi)^d} \frac{d^d k_2}{(2\pi)^d} \mathcal{A}_j(k_1, k_2) \mathcal{M}_{k_1, k_2}^{[LR]}(\ell_1, \ell_2) \mathcal{C}(k_1) \mathcal{C}(k_2), \quad (\text{B.1})$$

⁵To achieve NNLL accuracy in the resummed soft function Eq. (2.9) it is actually necessary to know the cusp anomalous dimension and beta function $\mathcal{O}(\alpha_s^3)$ as well, but in this paper we are only concerned with the fixed-order result.

where $\mathcal{C}(k)$ is the cut propagator, Eq. (3.5), we sum over the squared matrix elements from different classes of diagrams $\mathcal{A}_j = (\mathcal{I}, \mathcal{T}, \mathcal{G}, \mathcal{H}, \mathcal{Q})$ (see Fig. 1), and the momentum space measurement function is

$$\begin{aligned} \mathcal{M}_{k_1, k_2}^{[LR]}(\ell_1, \ell_2) &= \delta(\ell_1 - k_1^-) \delta(\ell_2 - k_2^+) \theta(k_1^+ - k_1^-) \theta(k_2^- - k_2^+) \\ &\quad + \delta(\ell_1 - k_2^-) \delta(\ell_2 - k_1^+) \theta(k_1^- - k_1^+) \theta(k_2^+ - k_2^-). \end{aligned}$$

The position space opposite hemisphere soft function is given by replacing the measurement function above by its position space analog, $\mathcal{M}_{k_1, k_2}^{[LR]}(x_1, x_2)$ in Eq. (3.12). More generally, the measurement function for other observables, \mathcal{M}_{k_1, k_2} , can be used with our results for the double cut squared matrix elements, \mathcal{A}_j , to obtain the contribution to the soft function for other observables.

The observable and hemisphere geometry sets some natural variables for the two loop calculation. The measurement function, and the diagrams, are symmetric in $k_1 \leftrightarrow k_2$, and therefore we focus only on the case where k_1 contributes to ℓ_1 and k_2 contributes to ℓ_2 . The initial matrix elements are straightforward to write in light cone coordinates, and the measurement function $\mathcal{M}_{k_1, k_2}^{[LR]}$ in Eq. (3.12) implements the conversion

$$k_1^- \rightarrow \ell_1, \quad k_2^+ \rightarrow \ell_2. \quad (\text{B.2})$$

It is natural to then scale out by these variables. We find that a pair of variables particularly useful for the calculations are

$$z \equiv \sqrt{\frac{k_1^+ k_2^-}{k_1^- k_2^+}} = \sqrt{\frac{k_1^+}{\ell_1} \frac{k_2^-}{\ell_2}}, \quad u \equiv \sqrt{\frac{k_1^+ / k_1^-}{k_2^- / k_2^+}} = \sqrt{\frac{k_1^+ \ell_2}{k_2^- \ell_1}}. \quad (\text{B.3})$$

The phase space cuts constrain $z > 1$, $u > 0$. Physically, the ratios k_1^+ / k_1^- and k_2^- / k_2^+ are related to the polar angles of the partons with respect to their jet directions. For example, $k_1^+ / k_1^- = \tan^2 \theta_1 / 2$, where θ_1 is the polar angle of the parton with respect to the jet (thrust) axis.

The z variable measures how close to the boundary the combination of the two partons are: as $z \rightarrow 1$, both partons move towards the hemisphere boundary, and as $z \rightarrow \infty$, the angular separation between the partons grows. u measures the relative angles of the two partons. It is worth noting that divergences from $z \rightarrow 1$ play a role in the appearance of non-global logarithms.

With the exception of the \mathcal{I} matrix elements that are straightforward to evaluate, we find a common set of transformations are useful to simplify the integral form of the matrix elements. The matrix elements depend on the set of variables

$$\{k_1^+, k_1^-, k_2^+, k_2^-, \phi\}, \quad (\text{B.4})$$

where ϕ is the angle between k_1 and k_2 in the plane transverse to the thrust axis. Our matrix elements depend only on $\cos \phi$, which arises from $k_1^\perp \cdot k_2^\perp$. Starting with the two

loop measure, we can perform some of the integrals to obtain

$$\int \frac{d^d k_1}{(2\pi)^d} \frac{d^d k_2}{(2\pi)^d} \mathcal{C}(k_1) \mathcal{C}(k_2) = \frac{1}{(16\pi^2)^2} \frac{(e^{\gamma_E})^{2\epsilon}}{\Gamma(1-\epsilon)^2} \int_0^\infty dk_1^+ dk_1^- dk_2^+ dk_2^- (k_1^+ k_1^- k_2^+ k_2^-)^{-\epsilon} \\ \times \left(\frac{\pi^{1/2} \Gamma(\frac{1}{2} - \epsilon)}{\Gamma(1-\epsilon)} \right)^{-1} \int_0^\pi d\phi \sin^{-2\epsilon} \phi. \quad (\text{B.5})$$

The measurement function then allows us to perform the k_1^- and k_2^+ integrals. For the opposite hemisphere contributions shifting to z and u requires the change of variables

$$\int_0^\infty \frac{dk_1^+}{k_1^-} \frac{dk_2^-}{k_2^+} \theta(k_1^+ > k_1^-) \theta(k_2^- > k_2^+) = \int_1^\infty dz \int_{1/z}^z du \frac{2z}{u}. \quad (\text{B.6})$$

This change of variables is convenient because in all the diagrams the u integration is independent of ϵ and can be easily performed. Additionally, the ϕ dependent terms in the matrix elements, which give hypergeometric functions when integrated, are independent of u . This means that we can simultaneously perform the u and ϕ integrals, making each diagram a single integral over z . Standard techniques can then be used to evaluate these z integrals.

In addition to a common strategy for evaluating the integrals, several common functions arise in the calculation. Using the z, u variables, a function of r that appears is nearly all the diagrams is

$$g(z, r) \equiv \ln \left(\frac{(1+r)^2 z}{(z+r)(1+rz)} \right). \quad (\text{B.7})$$

This function is symmetric in $r \rightarrow 1/r$ and scales as r for small r . In addition, there are two common hypergeometric functions that arise from integrations over ϕ :

$$\left(\frac{\pi^{1/2} \Gamma(\frac{1}{2} - \epsilon)}{\Gamma(1-\epsilon)} \right)^{-1} \int_0^\pi d\phi \sin^{-2\epsilon} \phi \frac{1}{1+z^2-2z \cos \phi} = \frac{1}{z^2+1} f_1(z^2), \quad (\text{B.8}) \\ \left(\frac{\pi^{1/2} \Gamma(\frac{1}{2} - \epsilon)}{\Gamma(1-\epsilon)} \right)^{-1} \int_0^\pi d\phi \sin^{-2\epsilon} \phi \frac{1}{(1+z^2-2z \cos \phi)^2} = -\frac{1}{(z^2+1)^2} [f_1(z^2) - 2f_2(z^2)],$$

where

$$f_1(z) \equiv {}_2F_1 \left(\frac{1}{2}, 1, 1-\epsilon, \frac{4z}{(1+z)^2} \right), \\ f_2(z) \equiv {}_2F_1 \left(\frac{1}{2}, 2, 1-\epsilon, \frac{4z}{(1+z)^2} \right). \quad (\text{B.9})$$

It is necessary to expand these functions to $\mathcal{O}(\epsilon^2)$:

$$f_1(z) = (1+z) z^{2\epsilon} (z-1)^{-1-2\epsilon} [1 + 2\epsilon^2 \text{Li}_2(1/z)] + \mathcal{O}(\epsilon^3), \\ f_2(z) = (1+z) z^{2\epsilon} (z-1)^{-3-2\epsilon} \left[1 + z^2 + 2\epsilon(1+z) \right. \\ \left. - 2\epsilon^2(z^2-1) \ln \left(\frac{z-1}{z} \right) + 2\epsilon^2(1+z^2) \text{Li}_2 \left(\frac{1}{z} \right) \right] + \mathcal{O}(\epsilon^3) \quad (\text{B.10})$$

Note that we have summed up terms at higher orders in ϵ in these expansions. Throughout the calculation we made use of the `HypExp` package [51, 52]. The divergent structure in ϵ of the vacuum polarization diagrams is quite complex, and careful treatment is necessary to ensure the divergences are regulated and terms are not forgotten. The difficulty in evaluating these diagrams comes from the hypergeometrics; using certain hypergeometric forms we can see more clearly the regulation of the divergences in the integrand about $z = 1$.

B.1 Form of the Matrix Elements in Momentum and Position Space

Before giving results for the matrix elements, we discuss the general form of the soft function. We determine the matrix elements in both momentum and position space. In position space the soft function is a simple function of the variables x_1 and x_2 , which are conjugate to ℓ_1, ℓ_2 . In momentum space the ℓ_1, ℓ_2 dependence gives distributions (rather than functions), but the result does not take a simple form in these variables. Instead, we use variables

$$s = \ell_1 \ell_2, \quad r = \frac{\ell_2}{\ell_1}, \quad \int_0^\infty d\ell_1 d\ell_2 = \int_0^\infty ds dr \frac{1}{2r}. \quad (\text{B.11})$$

The distributions in terms of these variables is simple: all matrix elements contain a distribution of s and non-singular functions of r . The general form of the opposite hemisphere terms in momentum space is

$$S^{\text{OPP}}(\ell_1, \ell_2) = \sum_i S^{\text{OPP}[i]}(\ell_1, \ell_2), \quad (\text{B.12})$$

where

$$S^{\text{OPP}[i]}(\ell_1, \ell_2) = A C_i s^{-1-2\epsilon} \mathcal{F}(r) \quad (\text{B.13})$$

and C_i is a color structure, (C_F^2 , $C_F C_A$, or $C_F T_{Rn_f}$), F_0 and $F_1(r)$ depend on the class of diagram, ($\mathcal{I}, \mathcal{T}, \mathcal{G}, \mathcal{H}, \mathcal{Q}$), and in $\overline{\text{MS}}$

$$A \equiv \left(\frac{\alpha_s}{2\pi}\right)^2 \frac{(e^{\gamma_E} \mu^2)^{2\epsilon}}{\Gamma(1-\epsilon)^2}. \quad (\text{B.14})$$

The relation to the position space matrix element is

$$S^{\text{OPP}[i]}(x_1, x_2) = A C_i \int_0^\infty ds dr \frac{1}{2r} e^{-i\sqrt{s}(x_1/\sqrt{r}+x_2\sqrt{r})} s^{-1-2\epsilon} \mathcal{F}(r). \quad (\text{B.15})$$

Convergence of the Fourier transform requires $x_{1,2}$ to have a small negative imaginary component:

$$x_1 - i0^+, \quad x_2 - i0^+. \quad (\text{B.16})$$

Because both s and r are positive, the sign of $i0^+$ relative to $x_{1,2}$ is unchanged for the entire Fourier transform. We will often write just $x_{1,2}$ with the prescription in Eq. (B.16) implied.

In all matrix elements the function $\mathcal{F}(r)$ is non-singular, meaning it can be split into a pure constant plus a nontrivial function of r ,

$$\mathcal{F}(r) = F_0 + F_1(r), \quad (\text{B.17})$$

where $F_1(r)$ is symmetric in $r \rightarrow 1/r$, and vanishes as $r \rightarrow 0, \infty$. The s integral can be done immediately, giving

$$S^{\text{opp}[i]}(x_1, x_2) = AC_i \Gamma(-4\epsilon) \int_0^\infty \frac{dr}{r} [F_0 + F_1(r)] \left[i \left(\frac{x_1}{\sqrt{r}} + x_2 \sqrt{r} \right) \right]^{4\epsilon}. \quad (\text{B.18})$$

The r integral in the F_0 piece can also be done immediately, using

$$\int_0^\infty \frac{dr}{r} \left[i \left(\frac{x_1}{\sqrt{r}} + x_2 \sqrt{r} \right) \right]^{4\epsilon} = (ix_1 ix_2)^{2\epsilon} \frac{\Gamma(-2\epsilon)^2}{\Gamma(-4\epsilon)}. \quad (\text{B.19})$$

Then each contribution to the opposite hemisphere soft function can be written

$$S^{\text{opp}[i]}(x_1, x_2) = AC_i (ix_1 ix_2)^{2\epsilon} \left\{ \Gamma(-2\epsilon)^2 F_0 + \Gamma(-4\epsilon) \int_0^\infty \frac{dr}{r} F_1(r) \left(\sqrt{\frac{b}{r}} + \sqrt{\frac{r}{b}} \right)^{4\epsilon} \right\}, \quad (\text{B.20})$$

where

$$b \equiv \frac{x_1 - i0^+}{x_2 - i0^+}. \quad (\text{B.21})$$

The function $F_1(r)$ always vanishes sufficiently quickly at $r \rightarrow 0, \infty$ so that the r integral introduces no additional powers of $1/\epsilon$, and thus the integrand can be expanded and truncated at $\mathcal{O}(\epsilon)$. Splitting the integral into the regions $0 < r < 1$ and $1 < r < \infty$, and using the symmetry of $F_1(r)$ in $r \rightarrow 1/r$, we can rewrite the last integral as

$$\int_0^1 \frac{dr}{r} F_1(r) \left[2 + 4\epsilon \ln \left(r + \frac{1}{r} + b + \frac{1}{b} \right) + \mathcal{O}(\epsilon^2) \right]. \quad (\text{B.22})$$

The last integral displays logarithmic dependence on b and $1/b$, which can be extracted by

$$\ln \left(r + \frac{1}{r} + b + \frac{1}{b} \right) = \ln \left(2 + b + \frac{1}{b} \right) + \ln \left(\frac{r + \frac{1}{r} + b + \frac{1}{b}}{2 + b + \frac{1}{b}} \right). \quad (\text{B.23})$$

Then Eq. (B.20) can be written

$$S^{\text{opp}[i]}(x_1, x_2) = AC_i (ix_1 ix_2)^{2\epsilon} \left\{ \Gamma(-2\epsilon)^2 F_0 + \Gamma(-4\epsilon) \left[2 + 4\epsilon \ln \left(2 + b + \frac{1}{b} \right) \right] \int_0^1 \frac{dr}{r} F_1(r) + 4\epsilon \Gamma(-4\epsilon) \int_0^1 \frac{dr}{r} F_1(r) \ln \left(\frac{r + \frac{1}{r} + b + \frac{1}{b}}{2 + b + \frac{1}{b}} \right) \right\}. \quad (\text{B.24})$$

In each term, the $F_{0,1}$ also have expansions in ϵ , and should be kept/truncated to the appropriate order. In particular, we must keep terms of up to order ϵ^2 in F_0 , but only to order ϵ in $F_1(r)$ (and only ϵ^0 in the last integral). Note that in the last integral the integrand now vanishes at both endpoints, $r \rightarrow 0$ (due to $F_1(r)$) and $r \rightarrow 1$ (due to the log).

We now give the result for each group of diagrams in both position and momentum space, as well as the intermediate step where only the z integral remains.

B.2 \mathcal{I} and \mathcal{T} diagrams

The matrix element for the C_F^2 diagrams is

$$\mathcal{A}_{\mathcal{I}, C_F^2} = 8g^4 \mu^{4\epsilon} C_F^2 \frac{1}{k_1^+ k_1^-} \frac{1}{k_2^+ k_2^-}, \quad (\text{B.25})$$

This diagram is the product of one loop diagrams with one gluon in each hemisphere (neglecting the delta function in the one loop diagrams for the hemisphere with no parton). In position space, the result of the diagram is

$$\tilde{\mathcal{I}}_{C_F^2} = A C_F^2 (ix_1 ix_2)^{2\epsilon} \Gamma(-2\epsilon)^2 \frac{4}{\epsilon^2}. \quad (\text{B.26})$$

The result in momentum space is

$$\mathcal{I}_{C_F^2} = A C_F^2 (\ell_1 \ell_2)^{-1-2\epsilon} \frac{4}{\epsilon^2}. \quad (\text{B.27})$$

The matrix element for the $C_F C_A$ diagrams is

$$\mathcal{A}_{\mathcal{I}, C_F C_A} = -2g^4 C_F C_A \mu^{4\epsilon} \frac{(k_1^+ + k_2^+)(k_1^- + k_2^-) + k_1^+ k_1^- + k_2^+ k_2^-}{(k_1^+ + k_2^+)(k_1^- + k_2^-) k_1^+ k_1^- k_2^+ k_2^-}. \quad (\text{B.28})$$

To evaluate this diagram we use the variables $u = k_1^+ / k_2^+$ and $v = k_2^- / k_1^-$. An intermediate step in the calculation is

$$\mathcal{I}_{C_F C_A} = -A C_F C_A s^{-1-2\epsilon} \left[\frac{1}{\epsilon^2} + \int_{1/r}^{\infty} du \int_r^{\infty} dv (uv)^{-1-\epsilon} \frac{u+v}{(1+u)(1+v)} \right]. \quad (\text{B.29})$$

These integrals can be evaluated exactly in ϵ . The leading divergences in $\mathcal{I}_{C_F C_A}$ cancel with the \mathcal{T} diagrams, so we present the results for the sum of the diagrams.

The matrix element for the \mathcal{T} diagrams is

$$\mathcal{A}_{\mathcal{T}} = 2g^4 C_F C_A \mu^{4\epsilon} \frac{k_1^+ k_2^- + k_1^- k_2^+}{2k_1 \cdot k_2} \left[1 + \frac{k_1^+ k_1^- + k_2^+ k_2^-}{(k_1^+ + k_2^+)(k_1^- + k_2^-)} \right] \frac{1}{k_1^+ k_1^- k_2^+ k_2^-}. \quad (\text{B.30})$$

Using the variables and transformations described in Eqs. (B.2) – (B.10), the intermediate step in the calculation with the remaining z integral is

$$\mathcal{T} = A C_F C_A s^{-1-2\epsilon} \int_1^{\infty} dz z^{-1-\epsilon} f_1(z) \left[2 \ln z + \frac{z+1}{z-1} g(z, r) \right]. \quad (\text{B.31})$$

Since the leading divergences in the $\mathcal{I}_{C_F C_A}$ and \mathcal{T} diagrams cancel, we sum them. In position space, the result is

$$\begin{aligned} \tilde{\mathcal{I}}_{C_F C_A} + \tilde{\mathcal{T}} &= A C_F C_A (ix_1 ix_2)^{2\epsilon} \left\{ \Gamma(-2\epsilon)^2 \left(\frac{2\pi^2}{3} + 4\zeta_3 \epsilon + \frac{14\pi^4}{45} \epsilon^2 \right) \right. \\ &\quad + 4\Gamma(-4\epsilon) \left[\zeta_3 - \frac{\pi^2}{3} - 2\epsilon \left(\zeta_3 + \frac{\pi^4}{45} - \frac{\pi^2}{3} \right) \right] \\ &\quad \left. + \left(\frac{2\pi^2}{3} - 2\zeta_3 \right) \ln \left(2 + \frac{x_1}{x_2} + \frac{x_2}{x_1} \right) + \tilde{\mathcal{F}}_{\mathcal{I}\mathcal{T}} \left(\frac{x_1}{x_2} \right) + \tilde{\mathcal{F}}_{\mathcal{T}\mathcal{I}} \left(\frac{x_2}{x_1} \right) \right\}, \quad (\text{B.32}) \end{aligned}$$

where the last two terms are given by the integral

$$\begin{aligned}
F_{IT}(b) &\equiv \int_0^1 \frac{dr}{r} \ln \left(\frac{r + \frac{1}{r} + b + \frac{1}{b}}{2 + b + \frac{1}{b}} \right) \left[\frac{4 \ln(1+r)}{1+r} + \frac{4 \ln \left(1 + \frac{1}{r}\right)}{1 + \frac{1}{r}} - 2 \ln(1+r) \ln \left(1 + \frac{1}{r}\right) \right] \\
&= \tilde{\mathcal{F}}_{IT}(b) + \tilde{\mathcal{F}}_{IT}(1/b)
\end{aligned} \tag{B.33}$$

where

$$\begin{aligned}
\tilde{\mathcal{F}}_{IT}(b) &\equiv -\frac{\pi^4}{36} + \frac{\ln^4 b}{24} + \left(2\zeta_3 - \frac{2\pi^2}{3} \right) \ln(1+b) - \ln^2 b \ln(1-b) - \frac{\pi^2}{3} \text{Li}_2(1-b) \\
&\quad - 4 \ln b \text{Li}_2(b) + (\text{Li}_2(1-b))^2 + 6 \text{Li}_3(b) + 2 \ln b \text{Li}_3(1-b).
\end{aligned} \tag{B.34}$$

The sum of the two terms $F_{IT}(b) = \tilde{\mathcal{F}}_{IT}(b) + \tilde{\mathcal{F}}_{IT}(1/b)$ is a finite function of b , in fact vanishing as $b \rightarrow 0$ or $b \rightarrow \infty$.

In momentum space, the result can be written

$$\mathcal{I}_{C_F C_A} + \mathcal{T} = A C_F C_A s^{-1-2\epsilon} \left\{ \frac{2\pi^2}{3} + 4\zeta_3 \epsilon + \frac{14\pi^2}{45} \epsilon^2 + \hat{\mathcal{F}}_{IT}(r) + \hat{\mathcal{F}}_{IT}(1/r) \right\} \tag{B.35}$$

where

$$\begin{aligned}
\hat{\mathcal{F}}_{IT}(r) &\equiv \ln(1+r) \ln \left(1 + \frac{1}{r}\right) - \frac{4}{1+r} \ln(1+r) \\
&\quad - \epsilon \left[\frac{\pi^2}{3} - 3 \text{Li}_3(-r) - \frac{4}{1+r} \ln r + \left(\frac{4r}{1+r} + 2 \ln r \right) \text{Li}_2(-r) \right. \\
&\quad \left. + \left(\frac{1}{2} \ln^2 r - 2 \frac{1-r}{1+r} \ln r - 4 - \frac{\pi^2}{6} \right) \ln(1+r) \right],
\end{aligned} \tag{B.36}$$

The r -dependent functions appearing in Eq. (B.35) are the $\mathcal{I}_{C_F C_A} + \mathcal{T}$ contribution to the function $F_1(r)$ defined in Eq. (B.17). This contribution is explicitly symmetric in $r \rightarrow \frac{1}{r}$ and vanishes as $r \rightarrow 0$ or $r \rightarrow \infty$, as advertised. This is also true of the other diagrams, which have the same form.

B.3 \mathcal{G} and \mathcal{H} diagrams

The matrix element for the \mathcal{G} diagrams is

$$\begin{aligned}
\mathcal{A}_{\mathcal{G}} &= g^4 C_F C_A \mu^{4\epsilon} \frac{1}{(2k_1 \cdot k_2)^2 (k_1^+ + k_2^+)^2 (k_1^- + k_2^-)^2} \\
&\quad \left\{ (k_1^+ + k_2^+)(k_1^- + k_2^-) \left[-16k_1 \cdot k_2 - 2(1-\epsilon)(k_1^+ - k_2^+)(k_1^- - k_2^-) + 4(k_1^+ + k_2^+)(k_1^- + k_2^-) \right. \right. \\
&\quad \left. \left. + k_1^+ k_2^- + k_1^- k_2^+ \right] + (k_1^- + k_2^-)^2 \left[(1-\epsilon)(k_1^+ - k_2^+)^2 - 2(k_1^+ + k_2^+)^2 - k_1^+ k_2^+ \right] \right. \\
&\quad \left. + (k_1^+ + k_2^+)^2 \left[(1-\epsilon)(k_1^- - k_2^-)^2 - 2(k_1^- + k_2^-)^2 - k_1^- k_2^- \right] \right\}.
\end{aligned} \tag{B.37}$$

The matrix element for the \mathcal{H} diagrams is

$$\begin{aligned}
\mathcal{A}_{\mathcal{H}} &= g^4 C_F C_A \mu^{4\epsilon} \frac{1}{(2k_1 \cdot k_2)^2 (k_1^+ + k_2^+)^2 (k_1^- + k_2^-)^2} \\
&\quad \times \left\{ -(k_1^+ + k_2^+)(k_1^- + k_2^-) (k_1^+ k_2^- + k_1^- k_2^+) + k_1^+ k_2^+ (k_1^- + k_2^-)^2 + k_1^- k_2^- (k_1^+ + k_2^+)^2 \right\}.
\end{aligned} \tag{B.38}$$

The ghost loop diagram cancels a set of terms in the gluon loop diagram, and so we evaluate them together. Using the variables and transformations described in Eqs. (B.2) – (B.10), the intermediate step in the calculation with the remaining z integral is

$$\mathcal{G} + \mathcal{H} = A C_F C_A s^{-1-2\epsilon} \int_1^\infty dz z^{-\epsilon} \left\{ 4 \frac{1}{z^2-1} g(z, r) f_1(z) + 2(1-\epsilon) \frac{1}{z^2-1} g(z, r) [f_1(z) - 2f_2(z)] \right. \\ \left. + 2(1-\epsilon) \frac{z-1}{z+1} \frac{r}{(r+z)(1+rz)} [f_1(z) - 2f_2(z)] \right\}. \quad (\text{B.39})$$

In position space, the result is

$$\tilde{\mathcal{G}} + \tilde{\mathcal{H}} = A C_F C_A (ix_1 ix_2)^{2\epsilon} \left\{ \Gamma(-4\epsilon) \left(\frac{2}{3} - \frac{10\pi^2}{9} \right) + \left(\frac{10}{9} - \frac{31\pi^2}{54} + \frac{5}{3} \zeta_3 \right) \right. \\ \left. + \left(-\frac{1}{3} + \frac{5\pi^2}{9} \right) \ln \left(2 + \frac{x_1}{x_2} + \frac{x_2}{x_1} \right) + \tilde{\mathcal{F}}_{\mathcal{GH}} \left(\frac{x_1}{x_2} \right) + \tilde{\mathcal{F}}_{\mathcal{GH}} \left(\frac{x_2}{x_1} \right) \right\}, \quad (\text{B.40})$$

where the last two terms are given by the integral

$$F_{GH}(b) \equiv \int_0^1 \frac{dr}{r} \ln \left(\frac{r + \frac{1}{r} + b + \frac{1}{b}}{2 + b + \frac{1}{b}} \right) \frac{2}{3(1+r)^3} \quad (\text{B.41}) \\ \times \left[-2r(1+r) + (5+9r+6r^2) \ln(1+r) + (6r+9r^2+5r^3) \ln \left(1 + \frac{1}{r} \right) \right] \\ = \tilde{\mathcal{F}}_{\mathcal{GH}}(b) + \tilde{\mathcal{F}}_{\mathcal{GH}}(1/b),$$

with

$$\tilde{\mathcal{F}}_{\mathcal{GH}}(b) \equiv \frac{1}{3(1-b)} \ln b + \frac{b}{6(b-1)^2} \ln^2 b + \left(\frac{1}{3} - \frac{5\pi^2}{9} \right) \ln(1+b) - \frac{5}{6} \ln^2 b \ln(1-b) \\ - \frac{10}{3} \ln b \text{Li}_2(b) + 5 \text{Li}_3(b). \quad (\text{B.42})$$

In momentum space, the diagram is

$$\mathcal{G} + \mathcal{H} = A C_F C_A s^{-1-2\epsilon} \left\{ \hat{\mathcal{F}}_{\mathcal{GH}}(r) + \hat{\mathcal{F}}_{\mathcal{GH}}(1/r) \right\} \quad (\text{B.43})$$

where

$$\hat{\mathcal{F}}_{\mathcal{GH}}(r) = -\frac{2}{3(1+r)^3} \left[-2r + (5+9r+6r^2) \ln(1+r) \right] \quad (\text{B.44}) \\ - \frac{2\epsilon}{3(1+r)^3} \left[\frac{16}{3} r + \frac{5\pi^2}{12} (1+r)^3 - \left(\frac{31}{3} + 23r + 8r^2 \right) \ln(1+r) \right. \\ \left. - \frac{1}{2} (5+3r-3r^2-5r^3) \ln^2(1+r) + (6r+9r^2+5r^3) \text{Li}_2(-r) \right].$$

B.4 \mathcal{Q} diagrams

The matrix element for the \mathcal{Q} diagrams is

$$\begin{aligned} \mathcal{A}_{\mathcal{Q}} &= 8g^4 C_F T_R n_f \mu^{4\epsilon} \frac{1}{(2k_1 \cdot k_2)^2 (k_1^+ + k_2^+)^2 (k_1^- + k_2^-)^2} \\ &\times [k_1^+ k_2^+ (k_1^- + k_2^-)^2 + k_1^- k_2^- (k_1^+ + k_2^+)^2 \\ &\quad + (2k_1 \cdot k_2 - k_1^+ k_2^- - k_1^- k_2^+) (k_1^+ + k_2^+) (k_1^- + k_2^-)] . \end{aligned} \quad (\text{B.45})$$

Using the variables and transformations described in Eqs. (B.2) – (B.10), an intermediate step in the calculation is

$$\begin{aligned} \mathcal{Q} &= A C_F T_R n_f s^{-1-\epsilon} \int_1^\infty dz z^{-\epsilon} \left\{ -8 \frac{1}{z^2 - 1} g(z, r) [f_1(z) - f_2(z)] \right. \\ &\quad \left. - 4 \frac{z-1}{z+1} \frac{r}{(r+z)(1+rz)} [f_1(z) - 2f_2(z)] \right\} . \end{aligned} \quad (\text{B.46})$$

In position space, the result is

$$\begin{aligned} \tilde{\mathcal{Q}} &= A C_F T_R n_f (ix_1 ix_2)^{2\epsilon} \left\{ \Gamma(-4\epsilon) \left(-\frac{4}{3} + \frac{8\pi^2}{9} \right) - \left(\frac{17}{9} - \frac{16\pi^2}{27} + \frac{4}{3} \zeta(3) \right) \right. \\ &\quad \left. - \left(\frac{4\pi^2}{9} - \frac{2}{3} \right) \ln \left(2 + \frac{x_1}{x_2} + \frac{x_2}{x_1} \right) + \tilde{\mathcal{F}}_{\mathcal{Q}} \left(\frac{x_1}{x_2} \right) + \tilde{\mathcal{F}}_{\mathcal{Q}} \left(\frac{x_2}{x_1} \right) \right\} , \end{aligned} \quad (\text{B.47})$$

where the last two terms are given by the integral

$$\begin{aligned} F_{\mathcal{Q}}(b) &\equiv \int_0^1 \frac{dr}{r} \ln \left(\frac{r + \frac{1}{r} + b + \frac{1}{b}}{2 + b + \frac{1}{b}} \right) \frac{-4}{3(1+r)^3} \\ &\quad \times \left[-2r(1+r) + (1+r)^3 \ln \left(2 + r + \frac{1}{r} \right) + (1-r^3) \ln r \right] \\ &= \tilde{\mathcal{F}}_{\mathcal{Q}}(b) + \tilde{\mathcal{F}}_{\mathcal{Q}}(1/b) \end{aligned} \quad (\text{B.48})$$

with

$$\begin{aligned} \tilde{\mathcal{F}}_{\mathcal{Q}}(b) &\equiv \frac{2}{3(b-1)} \ln b - \frac{b}{3(b-1)^2} \ln^2 b - \left(\frac{2}{3} - \frac{4\pi^2}{9} \right) \ln(1+b) \\ &\quad + \frac{2}{3} \ln^2 b \ln(1-b) + \frac{8}{3} \ln b \text{Li}_2(b) - 4 \text{Li}_3(b) . \end{aligned} \quad (\text{B.49})$$

In momentum space, the diagram is

$$\mathcal{Q} = A C_F T_R n_f s^{-1-2\epsilon} \left\{ \hat{\mathcal{F}}_{\mathcal{Q}}(r) + \hat{\mathcal{F}}_{\mathcal{Q}}(1/r) \right\} , \quad (\text{B.50})$$

where

$$\begin{aligned} \hat{\mathcal{F}}_{\mathcal{Q}}(r) &= \frac{4}{3(1+r)^3} [-2r + (1+r)^3 \ln(1+r) + \ln r] \\ &\quad + \frac{8\epsilon}{3(1+r)^3} \left[\frac{5}{3} r + \frac{\pi^2}{24} (1+r)^3 - \frac{1}{8} (1+r)^3 \ln^2 r \right. \\ &\quad \left. - \left(\frac{8}{3} + 7r + r^2 \right) \ln(1+r) + \frac{1}{2} (r^3 - 1) \left(\ln^2(1+r) + \text{Li}_2(-r) \right) \right] . \end{aligned} \quad (\text{B.51})$$

B.5 Total Opposite Hemisphere Soft Functions

Adding up the results in Eqs. (B.32), (B.40), and (B.47) the total opposite hemisphere soft function in position space is

$$\begin{aligned}
S^{\text{opp}}(x_1, x_2) = & \left(\frac{\alpha_s}{2\pi} \right)^2 \frac{(e^{\gamma_E} \mu^2)^{2\epsilon}}{\Gamma(1-\epsilon)^2} (ix_1 ix_2)^{2\epsilon} \left\{ \Gamma(-2\epsilon)^2 \left[C_F^2 \frac{4}{\epsilon^2} + C_F C_A \left(\frac{2\pi^2}{3} + 4\zeta_3 \epsilon + \frac{14\pi^2}{45} \epsilon^2 \right) \right] \right. \\
& + \left[2\Gamma(-4\epsilon) - \ln \left(2 + \frac{x_1}{x_2} + \frac{x_2}{x_1} \right) \right] \\
& \times \left[C_F C_A \left(\frac{1}{3} - \frac{11\pi^2}{9} + 2\zeta_3 + \epsilon \left(-\frac{20}{9} + \frac{67\pi^2}{27} - \frac{4\pi^4}{45} - \frac{22}{3} \zeta_3 \right) \right) \right. \\
& \quad \left. \left. + C_F T_{Rn_f} \left(-\frac{2}{3} + \frac{4\pi^2}{9} + \epsilon \left(\frac{34}{9} - \frac{32\pi^2}{27} + \frac{8}{3} \zeta_3 \right) \right) \right] \right\} \\
& + C_F C_A \left(\tilde{\mathcal{F}}_{C_F C_A} \left(\frac{x_2}{x_1} \right) + \tilde{\mathcal{F}}_{C_F C_A} \left(\frac{x_1}{x_2} \right) \right) \\
& + C_F T_{Rn_f} \left(\tilde{\mathcal{F}}_{C_F T_{Rn_f}} \left(\frac{x_2}{x_1} \right) + \tilde{\mathcal{F}}_{C_F T_{Rn_f}} \left(\frac{x_1}{x_2} \right) \right) \Bigg\}, \tag{B.52}
\end{aligned}$$

where

$$\tilde{\mathcal{F}}_{C_F C_A} \left(\frac{x_2}{x_1} \right) = \tilde{\mathcal{F}}_{IT} \left(\frac{x_2}{x_1} \right) + \tilde{\mathcal{F}}_{GH} \left(\frac{x_2}{x_1} \right), \tag{B.53}$$

which are given in Eqs. (B.34) and (B.42) and

$$\tilde{\mathcal{F}}_{C_F T_{Rn_f}} \left(\frac{x_2}{x_1} \right) = \tilde{\mathcal{F}}_{\mathcal{Q}} \left(\frac{x_2}{x_1} \right), \tag{B.54}$$

which is given in Eq. (B.49). In momentum space adding up the contributions from Eqs. (B.35), (B.43), and (B.50) the total opposite hemisphere soft function is

$$\begin{aligned}
S^{\text{opp}}(\ell_1, \ell_2) = & \left(\frac{\alpha_s}{2\pi} \right)^2 \frac{(e^{\gamma_E} \mu^2)^{2\epsilon}}{\Gamma(1-\epsilon)^2} C_F^2 (\ell_1 \ell_2)^{-1-2\epsilon} \frac{4}{\epsilon^2} \\
& + \left(\frac{\alpha_s}{2\pi} \right)^2 \frac{(e^{\gamma_E} \mu^2)^{2\epsilon}}{\Gamma(1-\epsilon)^2} (\ell_1 \ell_2)^{-1-2\epsilon} \left\{ C_F C_A \left(\frac{2\pi^2}{3} + 4\zeta_3 \epsilon + \frac{14\pi^2}{45} \epsilon^2 \right) \right. \\
& + C_F C_A \left[\hat{\mathcal{F}}_{IT}(r) + \hat{\mathcal{F}}_{IT}(1/r) + \hat{\mathcal{F}}_{GH}(r) + \hat{\mathcal{F}}_{GH}(1/r) \right] \\
& \left. + C_F T_{Rn_f} \left[\hat{\mathcal{F}}_{\mathcal{Q}}(r) + \hat{\mathcal{F}}_{\mathcal{Q}}(1/r) \right] \right\} \tag{B.55}
\end{aligned}$$

where $\hat{\mathcal{F}}_{IT}(r)$, $\hat{\mathcal{F}}_{GH}(r)$, and $\hat{\mathcal{F}}_{\mathcal{Q}}(r)$ are defined in Eqs. (B.36), (B.44), and (B.51), respectively.

References

- [1] G. Sterman, *Partons, factorization and resummation*, [hep-ph/9606312](#).
- [2] S. Catani, G. Turnock, B. R. Webber, and L. Trentadue, *Thrust distribution in e^+e^- annihilation*, *Phys. Lett.* **B263** (1991) 491–497.
- [3] S. Catani, L. Trentadue, G. Turnock, and B. R. Webber, *Resummation of large logarithms in e^+e^- event shape distributions*, *Nucl. Phys.* **B407** (1993) 3–42.
- [4] H. Contopanagos, E. Laenen, and G. Sterman, *Sudakov factorization and resummation*, *Nucl. Phys.* **B484** (1997) 303–330, [[hep-ph/9604313](#)].
- [5] C. W. Bauer, S. Fleming, and M. E. Luke, *Summing Sudakov logarithms in $B \rightarrow X_s \gamma$ in effective field theory*, *Phys. Rev.* **D63** (2000) 014006, [[hep-ph/0005275](#)].
- [6] C. W. Bauer, S. Fleming, D. Pirjol, and I. W. Stewart, *An effective field theory for collinear and soft gluons: Heavy to light decays*, *Phys. Rev.* **D63** (2001) 114020, [[hep-ph/0011336](#)].
- [7] C. W. Bauer and I. W. Stewart, *Invariant operators in collinear effective theory*, *Phys. Lett.* **B516** (2001) 134–142, [[hep-ph/0107001](#)].
- [8] C. W. Bauer, D. Pirjol, and I. W. Stewart, *Soft-collinear factorization in effective field theory*, *Phys. Rev.* **D65** (2002) 054022, [[hep-ph/0109045](#)].
- [9] C. W. Bauer, S. Fleming, D. Pirjol, I. Z. Rothstein, and I. W. Stewart, *Hard scattering factorization from effective field theory*, *Phys. Rev.* **D66** (2002) 014017, [[hep-ph/0202088](#)].
- [10] E. Farhi, *A QCD test for jets*, *Phys. Rev. Lett.* **39** (1977) 1587–1588.
- [11] L. Clavelli, *Jet invariant mass in quantum chromodynamics*, *Phys. Lett.* **B85** (1979) 111.
- [12] C. F. Berger, T. Kucs, and G. Sterman, *Event shape / energy flow correlations*, *Phys. Rev.* **D68** (2003) 014012, [[hep-ph/0303051](#)].
- [13] S. Fleming, A. H. Hoang, S. Mantry, and I. W. Stewart, *Jets from massive unstable particles: Top-mass determination*, *Phys. Rev.* **D77** (2008) 074010, [[hep-ph/0703207](#)].
- [14] M. D. Schwartz, *Resummation and NLO matching of event shapes with effective field theory*, *Phys. Rev.* **D77** (2008) 014026, [[arXiv:0709.2709](#)].
- [15] S. Fleming, A. H. Hoang, S. Mantry, and I. W. Stewart, *Top jets in the peak region: Factorization analysis with NLL resummation*, *Phys. Rev.* **D77** (2008) 114003, [[arXiv:0711.2079](#)].
- [16] T. Becher and M. D. Schwartz, *A precise determination of α_s from LEP thrust data using effective field theory*, *JHEP* **07** (2008) 034, [[arXiv:0803.0342](#)].
- [17] A. Hornig, C. Lee, and G. Ovanesyan, *Effective predictions of event shapes: Factorized, resummed, and gapped angularity distributions*, *JHEP* **05** (2009) 122, [[arXiv:0901.3780](#)].
- [18] R. Abbate, M. Fickinger, A. H. Hoang, V. Mateu, and I. W. Stewart, *Thrust at N^3LL with Power Corrections and a Precision Global Fit for $\alpha_s(m_Z)$* , *Phys. Rev.* **D83** (2011) 074021, [[arXiv:1006.3080](#)].
- [19] C. W. Bauer, S. Fleming, C. Lee, and G. Sterman, *Factorization of e^+e^- event shape distributions with hadronic final states in Soft Collinear Effective Theory*, *Phys. Rev.* **D78** (2008) 034027, [[arXiv:0801.4569](#)].

- [20] M. Dasgupta and G. P. Salam, *Resummation of non-global QCD observables*, *Phys. Lett.* **B512** (2001) 323–330, [[hep-ph/0104277](#)].
- [21] A. H. Hoang and S. Kluth, *Hemisphere soft function at $\mathcal{O}(\alpha_s^2)$ for dijet production in e^+e^- annihilation*, [arXiv:0806.3852](#).
- [22] Y.-T. Chien and M. D. Schwartz, *Resummation of heavy jet mass and comparison to LEP data*, *JHEP* **1008** (2010) 058, [[arXiv:1005.1644](#)].
- [23] S. Catani and M. H. Seymour, *The dipole formalism for the calculation of QCD jet cross sections at next-to-leading order*, *Phys. Lett.* **B378** (1996) 287–301, [[hep-ph/9602277](#)].
- [24] S. Catani and M. H. Seymour, *A general algorithm for calculating jet cross sections in NLO QCD*, *Nucl. Phys.* **B485** (1997) 291–419, [[hep-ph/9605323](#)].
- [25] I. W. Stewart, F. J. Tackmann, and W. J. Waalewijn, *Factorization at the LHC: From PDFs to Initial State Jets*, *Phys. Rev.* **D81** (2010) 094035, [[arXiv:0910.0467](#)].
- [26] I. W. Stewart, F. J. Tackmann, and W. J. Waalewijn, *N-Jettiness: An Inclusive Event Shape to Veto Jets*, *Phys. Rev. Lett.* **105** (2010) 092002, [[arXiv:1004.2489](#)].
- [27] M. Dasgupta, *On deglobalization in QCD*, *Pramana* **62** (2004) 675–678, [[hep-ph/0304086](#)].
- [28] S. D. Ellis, C. K. Vermilion, J. R. Walsh, A. Hornig, and C. Lee, *Jet Shapes and Jet Algorithms in SCET*, *JHEP* **11** (2010) 101, [[arXiv:1001.0014](#)].
- [29] A. Banfi, M. Dasgupta, K. Khelifa-Kerfa, and S. Marzani, *Non-global logarithms and jet algorithms in high- p_T jet shapes*, [arXiv:1004.3483](#).
- [30] M. Rubin, *Non-Global Logarithms in Filtered Jet Algorithms*, *JHEP* **05** (2010) 005, [[arXiv:1002.4557](#)].
- [31] S. Catani and L. Trentadue, *Inhibited Radiation Dynamics in QCD*, *Phys. Lett.* **B217** (1989) 539–544.
- [32] S. Catani and L. Trentadue, *Resummation of the QCD Perturbative Series for Hard Processes*, *Nucl. Phys.* **B327** (1989) 323.
- [33] G. P. Korchemsky and G. Marchesini, *Resummation of large infrared corrections using Wilson loops*, *Phys. Lett.* **B313** (1993) 433–440.
- [34] C. Balzereit, T. Mannel, and W. Kilian, *Evolution of the light-cone distribution function for a heavy quark*, *Phys. Rev.* **D58** (1998) 114029, [[hep-ph/9805297](#)].
- [35] T. Becher and M. Neubert, *Threshold resummation in momentum space from effective field theory*, *Phys. Rev. Lett.* **97** (2006) 082001, [[hep-ph/0605050](#)].
- [36] Z. Ligeti, I. W. Stewart, and F. J. Tackmann, *Treating the b quark distribution function with reliable uncertainties*, *Phys. Rev.* **D78** (2008) 114014, [[arXiv:0807.1926](#)].
- [37] P. F. Monni and G. Luisoni, “Resummation of large IR logarithms for the Thrust distribution.” Talk presented at Loopfest X, May 12–14, 2011, Northwestern University.
- [38] C. W. Bauer, C. Lee, A. V. Manohar, and M. B. Wise, *Enhanced nonperturbative effects in Z decays to hadrons*, *Phys. Rev.* **D70** (2004) 034014, [[hep-ph/0309278](#)].
- [39] A. H. Hoang and I. W. Stewart, *Designing gapped soft functions for jet production*, *Phys. Lett.* **B660** (2008) 483–493, [[arXiv:0709.3519](#)].

- [40] J. G. M. Gatheral, *Exponentiation of eikonal cross-sections in nonabelian gauge theories*, *Phys. Lett.* **B133** (1983) 90.
- [41] J. Frenkel and J. C. Taylor, *Nonabelian eikonal exponentiation*, *Nucl. Phys.* **B246** (1984) 231.
- [42] V. Mateu, R. Abbate, A. Hoang, M. D. Schwartz, and I. W. Stewart, “Status of HJM fits: towards a precise determination of $\alpha_s(M_Z)$.” Talk presented at SCET 2011 Workshop, March 6–8, 2011, Carnegie Mellon University.
- [43] G. Sterman, *Mass divergences in annihilation processes. II. Cancellation of divergences in cut vacuum polarization diagrams*, *Phys. Rev. D* **17** (1978) 2789.
- [44] A. Hornig, C. Lee, and G. Ovanesyan, *Infrared safety in factorized hard scattering cross-sections*, *Phys. Lett.* **B677** (2009) 272–277, [[arXiv:0901.1897](#)].
- [45] C. Lee, A. Hornig, I. W. Stewart, J. R. Walsh, and S. Zuberi, “Non-Global Logs in SCET.” Talk presented at SCET 2011 Workshop, March 6–8, 2011, Carnegie Mellon University.
- [46] R. Abbate, M. Fickinger, A. Hoang, V. Mateu, and I. W. Stewart, *Global Fit of $\alpha_s(m_Z)$ to Thrust at NNNLL Order with Power Corrections*, *PoS RADCOR2009* (2010) 040, [[arXiv:1004.4894](#)].
- [47] I. W. Stewart, F. J. Tackmann, and W. J. Waalewijn, *The Quark Beam Function at NNLL*, *JHEP* **09** (2010) 005, [[arXiv:1002.2213](#)].
- [48] R. Kelley, R. M. Schabinger, M. D. Schwartz, and H. X. Zhu, *The two-loop hemisphere soft function*, [arXiv:1105.3676](#).
- [49] G. P. Korchemsky and A. V. Radyushkin, *Renormalization of the Wilson loops beyond the leading order*, *Nucl. Phys.* **B283** (1987) 342–364.
- [50] I. Korchemskaya and G. Korchemsky, *On lightlike Wilson loops*, *Phys.Lett.* **B287** (1992) 169–175.
- [51] T. Huber and D. Maitre, *HypExp: A Mathematica package for expanding hypergeometric functions around integer-valued parameters*, *Comput.Phys.Commun.* **175** (2006) 122–144, [[hep-ph/0507094](#)].
- [52] T. Huber and D. Maitre, *HypExp 2, Expanding Hypergeometric Functions about Half-Integer Parameters*, *Comput.Phys.Commun.* **178** (2008) 755–776, [[arXiv:0708.2443](#)].

This figure "NGLdistCFCA.png" is available in "png" format from:

<http://arxiv.org/ps/1105.4628v1>

This figure "NGLdistCFCAserrors.png" is available in "png" format from:

<http://arxiv.org/ps/1105.4628v1>

This figure "NGLdistCFNF.png" is available in "png" format from:

<http://arxiv.org/ps/1105.4628v1>

This figure "NGLdoublelogCFCA.png" is available in "png" format from:

<http://arxiv.org/ps/1105.4628v1>

This figure "NGLglobalCFNF.png" is available in "png" format from:

<http://arxiv.org/ps/1105.4628v1>